nature communications

Article

https://doi.org/10.1038/s41467-024-54191-4

ReaL-MGE is a tool for enhanced multiplex genome engineering and application to malonyl-CoA anabolism

Received: 26 March 2024

Accepted: 1 November 2024

Published online: 12 November 2024

Check for updates

Wentao Zheng[1,2,3,8], Yuxuan Wang[1,8], Jie Cui[1,8], Guangyao Guo[4], Yufeng Li[1], Jin Hou[1], Qiang Tu[1], Yulong Yin[5], A. Francis Stewart[1,6,7] ✉, Youming Zhang[1] ✉, Xiaoying Bian[1] ✉ & Xue Wang[1] ✉

The complexities encountered in microbial metabolic engineering continue to elude prediction and design. Unravelling these complexities requires strategies that go beyond conventional genetics. Using multiplex mutagenesis with double stranded (ds) DNA, we extend the multiplex repertoire previously pioneered using single strand (ss) oligonucleotides. We present ReaL-MGE (Recombineering and Linear CRISPR/Cas9 assisted Multiplex Genome Engineering). ReaL-MGE enables precise manipulation of numerous large DNA sequences as demonstrated by the simultaneous insertion of multiple kilobase-scale sequences into *E. coli*, *Schlegelella brevitalea* and *Pseudomonas putida* genomes without any off-target errors. ReaL-MGE applications to enhance intracellular malonyl-CoA levels in these three genomes achieved 26-, 20-, and 13.5-fold elevations respectively, thereby promoting target polyketide yields by more than an order of magnitude. In a further round of ReaL-MGE, we adapt *S. brevitalea* to malonyl-CoA elevation utilizing a restricted carbon source (lignocellulose from straw) to realize production of the anti-cancer secondary metabolite, epothilone from lignocellulose. Multiplex mutagenesis with dsDNA enables the incorporation of lengthy segments that can fully encode additional functions. Additionally, the utilization of PCR to generate the dsDNAs brings flexible design advantages. ReaL-MGE presents strategic options in microbial metabolic engineering.

Microbial metabolic engineering is proving to be much more challenging than initially anticipated. Despite the common tenets of metabolism shared by all cellular life, diverse microbial physiologies present a plethora of variations as well as a vast diversity of secondary metabolites. Unraveling the complexities to harness the extraordinary potential of microbes as chemical factories requires more than standard genetics or intentional genome engineering[1–4]. Although reliable, the classical concept of biochemical pathways has been misleadingly simplistic. Many attempts to engineer microbial factories indicate that metabolisms are highly interconnected, multi-layered networks where

[1]State Key Laboratory of Microbial Technology, Shandong University, Qingdao, Shandong, P. R. China. [2]Suzhou Research Institute of Shandong University, Room607, Building B of NUSP, NO.388 Ruoshui Road, SIP, Suzhou, Jiangsu, P. R. China. [3]Shenzhen Research Institute of Shandong University, A301 Virtual University Park in South District of Shenzhen, Guangdong, P. R. China. [4]College of Biotechnology, Tianjin University of Science and Technology, Tianjin, P. R. China. [5]Yuelushan Laboratory, Changsha, China. [6]Genomics, Biotechnology Center, Center for Molecular and Cellular Bioengineering, Technische Universität Dresden, Tatzberg 47-51, Dresden, Germany. [7]School of Biotechnology and Biomolecular Sciences, University of New South Wales, Sydney, Australia. [8]These authors contributed equally: Wentao Zheng, Yuxuan Wang, Jie Cui. ✉e-mail: francis.stewart@tu-dresden.de; zhangyouming@sdu.edu.cn; bianxiaoying@sdu.edu.cn; wangxue@sdu.edu.cn

almost any alteration provokes unexpected consequences. Databases and genome-scale metabolic models have been created to understand the networks involved in metabolism, energy budget, reducing power, and stress tolerance, amongst other parameters. However, unpredicted consequences provoked by simultaneous perturbation of two or more genes or pathways highlight the difficulties in modeling these complex interconnected networks. In addition, because network regulation and growth are coupled, abnormal over- or under-expression of different pathways has led to disordered growth and suboptimal metabolite output despite informed forecasting and/or extensive testing by trial and error[5–9].

The complexities encountered in microbial metabolic engineering require strategies that go beyond the limitations of low throughput mutagenesis, even if aided by modeling or random selection strategies. Thereby the imperative for multiplex mutagenesis has arisen, which is primarily being developed in bacteria using recombineering and CRISPR strategies[10–12]. Recombineering is DNA engineering in bacteria using homologous recombination (HR) mediated by phage SSAPs (single-strand annealing proteins). Initially discovered in *E. coli* for double-strand DNA (dsDNA) HR mediated by the phage exonuclease/SSAP pairs, RecE/RecT from *rac* and Redα/Redβ from λ[13–15], it was subsequently discovered that the exonuclease in these monogamous protein-protein interaction pairs[16] is not required for HR with single-stranded oligonucleotides (ss-oligos)[17,18]. The ability of Redβ alone to mediate HR using ss-oligos was employed to establish the breakthrough multiplex strategy, MAGE (Multiplex Automated Genome Engineering)[19]. Multiplex mutagenesis with ss-oligos has subsequently been extended in several ways, including CoS-MAGE, pORTMAGE, TRMR (Traceable RMR), enhanced eMAGE and DIvERGE (Directed Evolution of Random Genomic Mutations)[12,20–24]. To extend multiplex genome engineering to include mutagenesis with dsDNA, we developed dReaMGE (dsDNA Recombineering-assisted Multiple Genome Engineering) by showing that multiple dsDNA HR events are enhanced by (i) protecting one end of the dsDNA HR substrate using phosphorothioate, (ii) manipulating the speed of DNA replication, most simply by adding a low concentration of dNTPs in the electroporation recovery media; and (iii) optimizing recovery time after electroporation. With dReaMGE, simultaneous insertions and deletions of multiple kilobase-scale sequences were achieved in *E. coli* and two different *Pseudomonad* hosts[25]. CRISPR/Cas9 is efficient and versatile for genome editing in various organisms, but its application for multiplex genome targeting in bacteria is limited by several factors, including the cytotoxicity of Cas9 expression[26], difficulties in simultaneously co-expressing multiple guides RNAs[27], and the lethality of unrepaired double-strand breaks because most bacteria lack the capacity for non-homologous end joining[28]. Consequently, in bacteria, Cas9 was first applied as a transiently expressed counterselection tool after the recombineering step to eliminate unmutated genomes by cleavage of the wild-type target[11,29–31].

Here, we report the fluent multiplex mutagenesis using dsDNAs employing concerted CRISPR-promoted recombineering and counterselection, manipulation of the exonuclease VII (ExoVII), and utilization of multiple linear gRNA gene cassettes to achieve simultaneous mutagenesis of multiple *E. coli*, *S. brevitalea* and *P. putida* genomic sites. We term the enhanced dsDNA strategy ReaL-MGE.

To validate the power of ReaL-MGE, we embrace one of the most important challenges in metabolic engineering. Malonyl-coenzyme A (malonyl-CoA) derivatives have substantial relevance for industrial production[32,33] mainly due to a central role in polyketide synthase (PKS) and fatty acid synthase (FAS) pathways, which along with non-ribosomal peptide synthase (NRPS) are the major bacterial secondary metabolite pathways[34,35]. PKSs are enzymes responsible for the biosynthesis of polyketides, which are a diverse class of secondary metabolites found in bacteria, fungi, plants, and some animals. These metabolites are crucial for producing various pharmaceutical compounds, flavors, fragrances, and pigments. Type III PKSs are typically involved in the synthesis of simple polyketides. Both RppA and RpALS are Type III PKSs that produce specific polyketide compounds used in pharmaceuticals[35]. NRPSs are large, multifunctional enzymes responsible for the biosynthesis of peptides, often with therapeutic properties. NRPSs are used in the production of a wide range of pharmaceuticals, including antibiotics, immunosuppressants, and anticancer agents. For example, epothilones and glidobactins are both NRPS-PKS hybrid compounds with anticancer properties[36,37] (Supplementary Table 2 and Supplementary Fig. 1). The intracellular availability of malonyl-CoA is often limited due to tight regulation and competition with cellular metabolism and growth[35,38]. To date, this important challenge has been embraced by metabolic engineering in *E. coli*, *Corynebacterium glutamicum,* and *S. cerevisiae* variously aimed at either increasing the supply of acetyl-CoA, enhancing the activity of acetyl-CoA carboxylases (ACC), or reducing the consumption of malonyl-CoA[39–44]. Further achievements require not only increasing malonyl-CoA availability but also enhancing the growth performance of the host[34,44,45].

To enhance malonyl-CoA expression and thereby validate ReaL-MGE, we apply a multi-dimensional strategy that includes (i) malonyl-CoA metabolic network engineering and (ii) transposon removal and genome reduction. In a single engineering round using *E. coli* BL21, we obtained an *E. coli* BL21 strain (*E. coli* BL21.C33) altered at 14 genomic sites that exhibited a 26-fold increase in malonyl-CoA availability and an 11.4-fold improvement in the heterologous expression yield of the type III PKS compound, alonsone. Using *Schlegelella brevitalea* DSM7029 (formerly known as *Polyangium brachysporum* DSM7029[46]) through two rounds of ReaL-MGE, we obtain an *S. brevitalea* DSM7029 strain (*S. brevitalea* DSM7029Δglb.21:: lignocellulose) altered at 29 genomic sites. The selected strain can use lignocellulose as the only carbon source, and the yield of the PKS/NRPS secondary metabolite, epothilone C/D, was increased 150-fold. Using *Pseudomonas putida*, through one round of ReaL-MGE, we obtained a strain (*P. putida*.C177) mutated at 11 genomic sites with malonyl-CoA levels increased 13.5-fold. Total genome sequencing reveals the high accuracy of the intended mutagenesis and that none of the selected *E. coli*, *S. brevitalea,* or *P. putida* strains showed any off-target mutagenesis. ReaL-MGE significantly develops bacterial multiplex genome engineering by improving HR and avoids problems such as selection marker dependence and difficulties in constructing multiple gRNA co-expression plasmids. The ReaL-MGE mediated multi-dimensional strategy can aid and inspire future efforts to construct bacterial cell factories more in line with requirements.

Results

Concerted Cas9-promoted counterselection enhances triple targeting in *E. coli* BL21

To enhance dReaMGE for multiplex dsDNA genome engineering, we explored several possibilities beginning with a strategy to implement CRISPR/Cas9 to promote both HR and counterselection. To counter Cas9 cytotoxicity, which in our hands is severe and does not require gRNA expression, we put Cas9 under the tightly regulated arabinose inducible pBAD promoter. Consequently, we put the Red operon under the rhamnose inducible pRHA promoter. Both operons were mounted on a pBBR1 plasmid, pBBR1-P_{Rha}-Redγβα-P_{BAD}-Cas9-Km (Fig. 1a).

Recently, in fungus, such as yeast and *Aspergillus*, the problem of co-expressing multiple gRNAs for single genome region editing was solved by the co-introduction of multiple short gRNA-expressing PCR fragments[47–49]. To test whether this approach can work in bacterial multiplex genome editing, we generated three different gRNA-expressing PCR fragments incorporating the J23119 promoter[50]. Different from previous reports of using gRNA-expressing PCR fragments, we included terminal phosphorothioates for adding stability

https://doi.org/10.1038/s41467-024-54191-4

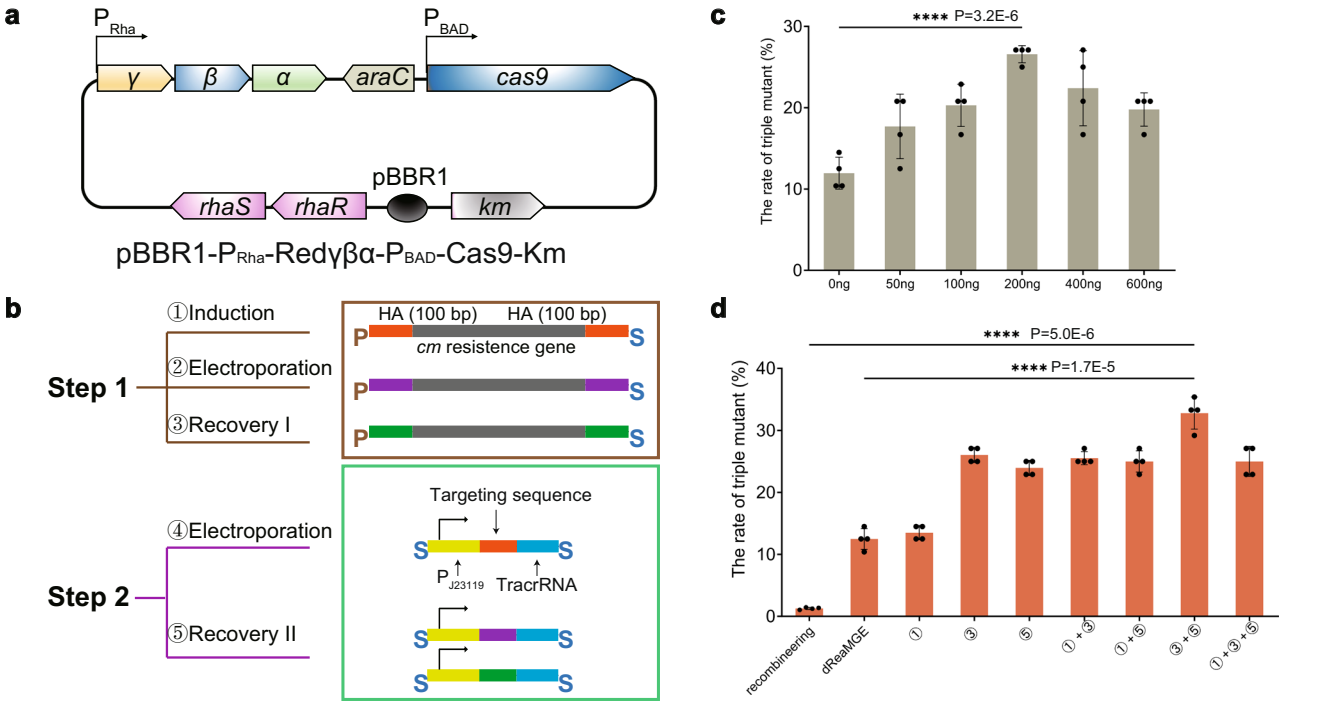

Fig. 1 | Addition of Cas9 expression and gRNA-expressing PCR fragments to dReaMGE in *E. coli* BL21. a The plasmid, pBBR1-P_{Rha}-Redγβα-P_{BAD}-Cas9-Km, was used for rhamnose induction of the Red operon (Redγ, β, α) and arabinose induction of Cas9. **b** The steps in the experiment are illustrated. Step 1: ① rhamnose induction; ② co-electroporation of three asymmetrically 5′ phosphorothioate dsDNA HR substrates (illustrated in the box with S denoting phosphorothioate, P denoting phosphorylation), each with 100 bp homology arms (red, purple or green denoting the different chosen genomic target sites); ③ addition of media for recovery in tube. Step 2: ④ co-electroporation of three gRNA-expressing PCR fragments protected by symmetrical 5′ phosphorothioate, each driven by the J23119 promoter; ⑤ addition of media for recovery in tube before plating. **c** Optimum titration of gRNA-expressing PCR fragments total input in Step 2 ($P = 0.0037$). **d** Examination of varied Cas9 expression by arabinose addition at the indicated points. Using 200 ng gRNA input, the addition of arabinose at ① delivered no improvement over dReaMGE. Arabinose addition in both recovery I ③ and II ⑤ delivered the most benefit for the triple mutation (2.6-fold compared to dReaMGE). Values are means of the biological replicates, and the error bars indicate the standard deviations of all ($n = 4$) biological replicates. *P* values were obtained using the two-tailed Student's *t* test: ****$P < 0.0001$.

against degradation, which was proved to be effective (Supplementary Fig. 2). In step 1, rhamnose induction of the Red operon was followed by co-electroporation of three linear, asymmetrically phosphorothioate, PCR-generated, HR substrates (Fig. 1b ① and ②). The Cas9 was induced to express in the recovery period after the first electroporation (Fig. 1b ③) followed by the second electroporation of various total inputs (0–600 ng) of three 5′ end phosphorothioate protected gRNA-expressing PCR fragments for counterselection (Fig. 1b ④), and finally an optimum total input of 200 ng was determined (Fig. 1c). To optimize the Cas9 expression profile for both HR and counterselection, arabinose was added at various times during the procedure. This revealed that arabinose addition in both recovery periods (Fig. 1b ③ and ⑤) delivered the triply mutated genome at the highest frequency (Fig. 1d). Consequently, a 2.6-fold enhancement in the efficacy of dReaMGE triple mutation was observed in *E. coli* BL21 using the chloramphenicol resistance gene (*cm*) as the sole selection marker, which illustrates the viability of co-introduction of multiple linear gRNA cassettes in *E. coli* BL21 (Fig. 1d).

Enhanced recombineering by ExoVII mutagenesis

In recombineering, one strand of a dsDNA HR substrate is completely removed by the partner exonuclease, and the remaining strand is annealed by the SSAP into the replication fork and then incorporated into the target by a subsequent round of replication[51]. Because the ssDNA intermediate is vulnerable to exonuclease degradation, the impact of various *E. coli* exonucleases on recombineering has been examined[52]. Here we highlight ExoVII, which has two kinds of subunits (one XseA subunit and four to six XseB subunits). ExoVII drew our attention because it was reported that ablation of *xseA* and overexpressing *xseB* can enhance the DNA repair ability of the host[53,54]. We investigated whether recombineering efficiency could be enhanced by *xseA* knock-out and *xseB* overexpression. For *xseB* overexpression, locating the *xseB* gene in the rhamnose inducible Red operon (pBBR1-P_{Rha}-Redγβα-xseB-Km; Fig. 2a) modestly improved the efficiency of recombineering (Fig. 2b). To delete the *xseA* gene, we established *E. coli* BL21*ΔxseA*, which also modestly enhanced recombineering efficiency (Fig. 2b). Notably, the combination of both *xseA* deletion and *xseB* overexpression promoted a three-fold enhancement than wild-type (from 7278 to 23293 /10^8 CFU) and a 1.4-fold enhancement than the *ΔxseA* mutant (from 16655 to 23293 /10^8 CFU) (Fig. 2b).

To further explore the effect of *xseA* knockout and *xseB* overexpression on recombineering, we also conducted experiments in *S. brevitalea* DSM7029 and *P. putida* KT2440. In these strains, overexpression of the host *xseB* gene, achieved by incorporating in the rhamnose-inducible recombinase operon (pBBR1-P_{Rha}-Redγ-Redβα7029-xseB7029-Km, pBBR1-P_{Rha}-BAS-xseBkt2440-Km; Fig. 2a), significantly improved recombineering efficiency by 2.2-fold for *S. brevitalea* DSM7029 and 3.1-fold for *P. putida* KT2440 (Fig. 2c, d). Similarly, deletion of the host *xseA* gene in these strains also led to a significant enhancement in recombineering efficiency by 2.3-fold for *S. brevitalea* DSM7029 and 2-fold for *P. putida* KT2440 (Fig. 2c, d). The *ΔxseA* + P-*xseB* system resulted in a 3.4-fold increase in recombineering efficiency in *S. brevitalea* DSM7029 (from 1281 to 3626 /10^8 CFU) and a 4.5-fold increase in *P. putida* KT2440 (from 1169 to 4761 /10^8 CFU; Fig. 2c, d). The *ΔxseA* + P-*xseB* system promoted a 1.3-fold increase in *S. brevitalea* DSM7029 *ΔxseA* mutant (from 2655 to 3626 /10^8 CFU) and a 1.8-fold increase in *P. putida* KT2440 *ΔxseA* mutant (from 2643 to 4761 /10^8 CFU; Fig. 2c, d). Therefore the strategy to overexpress *xseB* and

https://doi.org/10.1038/s41467-024-54191-4

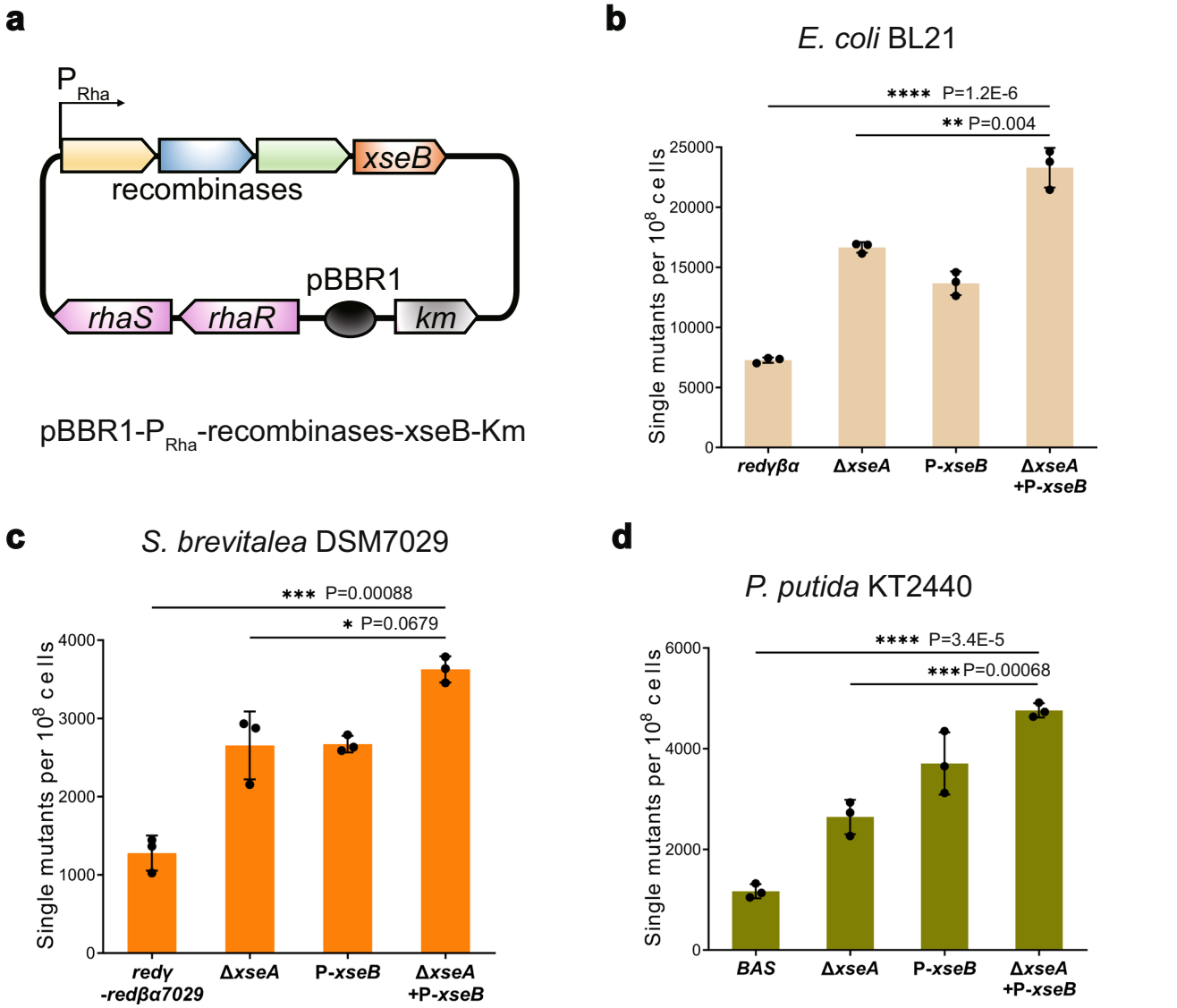

Fig. 2 | Manipulation of ExoVII improves homologous recombination in different bacteria. a Host's *xseB* gene was cloned into the recombinases to create pBBR1-P_{Rha}-recombinases-xseB-Km. **b** A conventional recombineering assay (insertion *cm* resistance gene into the genome using 100 bp homology arm) was used to evaluate the impact of the loss of *xseA* (*ΔxseA*), the overexpression of *xseB* (P-*xseB*) and combination of *ΔxseA* and P-*xse*B in *E. coli* BL21. **c** Manipulation of ExoVII in *S. brevitalea* DSM7029 (insertion of *genta* resistance gene into the genome using 100 bp homology arm). **d** Manipulation of ExoVII in *P. putida* KT2440 (insertion of *genta* resistance gene into the genome using 100 bp homology arm). Values are means of the biological replicates, and the error bars indicate the standard deviations of all ($n = 3$) biological replicates. *P*-values were obtained using the two-tailed Student's *t* test: $^{*}P < 0.1$, $^{**}P < 0.01$, $^{***}P < 0.001$, $^{****}P < 0.0001$.

knockout *xseA* is effective in enhancing recombineering efficiency in different bacterial strains.

Establishment of ReaL-MGE

To incorporate the XseB enhancement /*ΔxseA* into a portable multiplex dsDNA engineering strategy, we included an *xseA* inactivation cassette in pBBR1-P_{Rha}-Redγβα-xseB-P_{BAD}-Cas9-Km. This inactivation cassette included a gRNA-expressing region whose gRNA will direct Cas9 to (i) cleave the endogenous *xseA* gene and (ii) release a homology region to repair and mutate the Cas9 cleaved *xseA* gene (Fig. 3a). Five protocol variations were evaluated (Fig. 3b) all using the best procedure (that is, rhamnose induction for Redγβα-XseB expression before the first electroporation and arabinose induction for Cas9 expression in two recovery periods) accompanied by linear gRNA expressing PCR fragments. The asymmetrically phosphorothioated targeting substrate and symmetrically phosphorothioated gRNA-expressing fragments were variously electroporated at step 1 or step 2 as illustrated, including a variation where the two were physically linked by a target sequence for the encoded gRNA (Fig. 3b, iv and v). Of these variations, iv (now termed ReaL-MGE 1.0) delivered the greatest improvement to both single triple-mutagenesis, the efficiency of seamless single-mutagenesis mediated by ReaL-MGE 1.0 was 12.5 %, and efficiency of seamless triple-mutagenesis mediated by ReaL-MGE 1.0 was 0.6% (8 out of 1440), while recombineering, dReaMGE, dReaMGE plus and CREATE yielded no triple-mutants from similar numbers of transformants examined (Fig. 3c, d). ReaL-MGE 1.0 emerged as the most practical option for bacterial strains capable of tolerating the inherent cytotoxicity associated with the CRISPR/Cas9 system. Further description and a protocol for application of ReaL-MGE 1.0 in *E. coli* is detailed in Methods (**The establishment method of ReaL-MGE**).

The application of pBBR1-P_{Rha}-Redγ-Redβα7029-P_{BAD}-Cas9-Km in *S. brevitalea* DSM7029 encountered Cas9 toxicity, we could not transfer this plasmid into *S. brevitalea* DSM7029 even without arabinose induction (unpublished observations). The Cas9 toxicity has also been observed in *E. coli* BL21. The transient arabinose induction of

https://doi.org/10.1038/s41467-024-54191-4

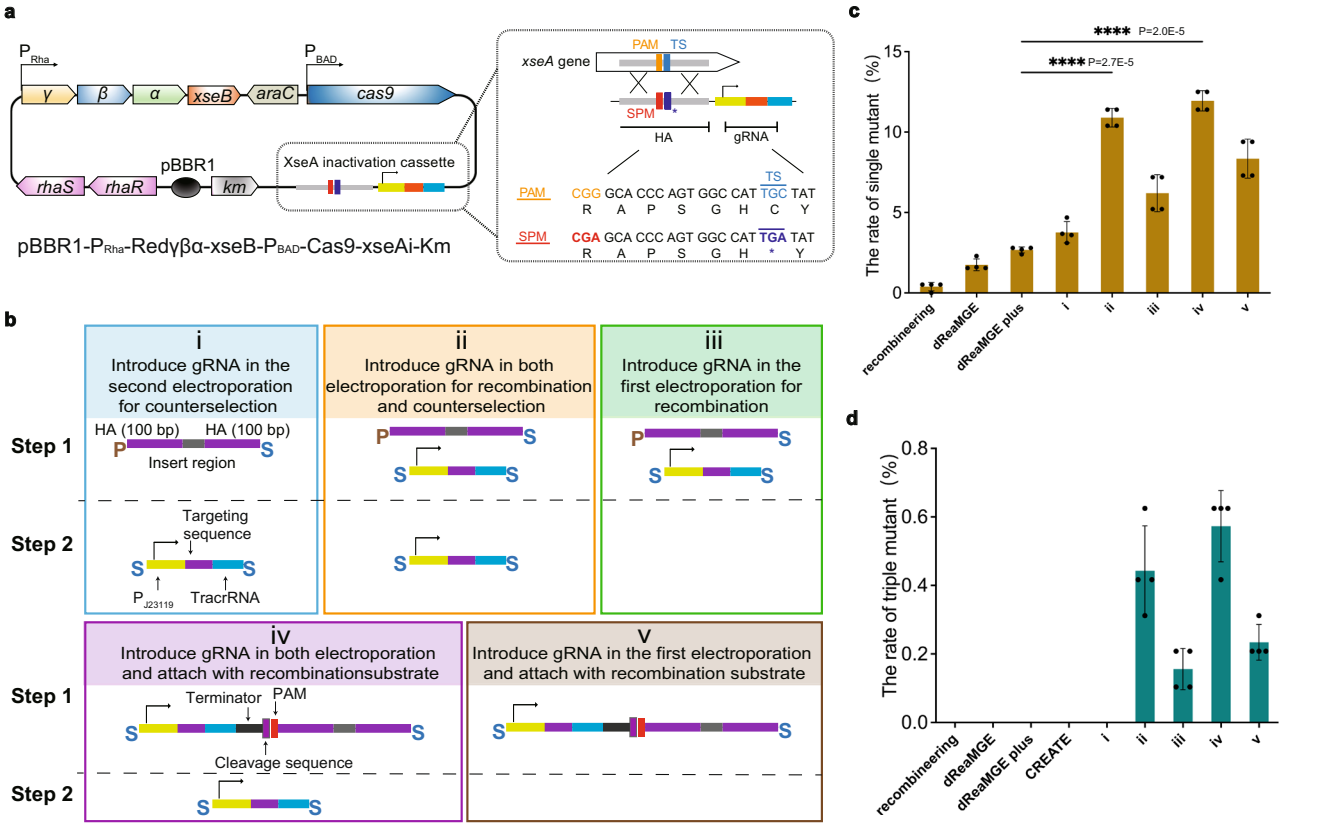

Fig. 3 | Establishment and utilization of ReaL-MGE 1.0 in *E. coli* BL21. a Diagram of pBBR1-P$_{Rha}$-Redγβα-xseB-P$_{BAD}$-Cas9-xseAi-Km, with details of the *xseA* inactivation cassette shown in the inset. The *xseA* gene in the genome is illustrated, including the target sequence (TS, blue) and inactive PAM version on the inactivation cassette (synonymous PAM mutation, SPM, red). **b** Five protocol variations (i – v) are illustrated based on twice electroporations with different combinations of gRNA-expressing PCR fragments and dsDNA substrates, arabinose induction was applied in two recovery periods. **c** Single-mutagenesis efficiencies (500 bp genomic region replaced by 230 bp dsDNA substrate) using different protocols as indicated, dReaMGE plus (dReaMGE with ExoVII exonuclease modified). **d** Triple mutagenesis efficiencies of *E. coli* using (i–v) and different dsDNA multiplex applications (dsDNA recombineering, dReaMGE, dReaMGE plus and CREATE). Values are means of the biological replicates, and the error bars indicate the standard deviations of all ($n = 4$) biological replicates. *P*-values were obtained using the two-tailed Student's *t* test: $^{****}P < 0.0001$.

Cas9 modestly repressed the growth of *E. coli* BL21 while the growth was unaffected without arabinose addition, suggesting the expression of Cas9 also has mildly toxicity on *E. coli* BL21 (Supplementary Fig. 3a). This motivated the development of a second approach based on using a linear Cas9 gene, which was PCR amplified from a template plasmid and linked to the gRNA gene (Fig. 4a). We beforehand evaluated other smaller RNA-guided endonucleases (enAsCas12a and AsCas12f1) and promoters to prefer P$_{genta}$-Cas9 for linear expression (Supplementary Fig. 3b, **c**). In addition, we explored the integration of three gRNAs using transfer RNA (tRNA) linkers[27,47]. However, this approach did not yield a significant enhancement in editing efficiency and introduced an additional experimental workload (Supplementary Fig. 4). Consequently, in subsequent investigations, we opted to express each gRNA individually on a single linear fragment. Using pBBR1-P$_{Rha}$-Redγβα-xseB-Km (Fig. 2a), five variations (vi to x) were evaluated in *E. coli* BL21 (Fig. 4b), with vii delivering the best outcome in the single-editing experiment (Fig. 4c). The efficiency of seamless triple-mutagenesis in *E. coli* BL21 mediated by vii was 0.3% (4 out of 1440), while recombineering, dReaMGE and CREATE yielded no triple-mutants from similar numbers of transformants examined (Fig. 4d). We term protocol vii, ReaL-MGE 2.0 and observed that it was strikingly effective in *S. brevitalea* DSM7029 for both single and triple mutagenesis (Fig. 4e). Further description and a protocol for application of ReaL-MGE 2.0 in *S. brevitalea* DSM7029 is also detailed in Methods (**The establishment method of ReaL-MGE**).

Multiplex malonyl-CoA metabolic and genome engineering in *E. coli*

Malonyl-CoA is synthesized from acetyl-CoA through the catalytic activity of acetyl-CoA carboxylase (ACC)[55]. Therefore, to elevate intracellular malonyl-CoA, elevating intracellular acetyl-CoA has been employed[40,41,43,44,56–59] including facilitated general carbon metabolism to elevate acetyl-CoA through elevated NAD(H), NADP(H$^+$), and ATP cofactor regeneration[60]. In this work, we aimed to elevate malonyl-CoA and also to incorporate our and others previous demonstration that deleting endogenous bacterial transposons, prophage sequences, and gene islands can lead to improved growth characteristics[61–66]. We used ReaL-MGE 1.0 to search for elevated malonyl-CoA in *E. coli* BL21 in the following way.

Twenty-one rate-limiting enzymes in nine malonyl-CoA synthetic or competing pathways were selected (Supplementary Table 3 and Supplementary Fig. 5a) for targeting with either (i) promoter replacement with the strong T7 promoter for increased expression (16 genes selected; Supplementary Fig. 5b), or (ii) the LVA protein degradation tag onto the C-terminus for decreased protein expression (5 genes selected; Supplementary Fig. 5c). Each of these targeted mutations was individually evaluated for malonyl-CoA levels, and each showed modest improvement (Supplementary Fig. 5d). All twenty-one mutations were then combined with the deletion of 5 transposases and 2 prophage sequences for concerted mutagenesis aimed at a total of 28 genome targets.

https://doi.org/10.1038/s41467-024-54191-4

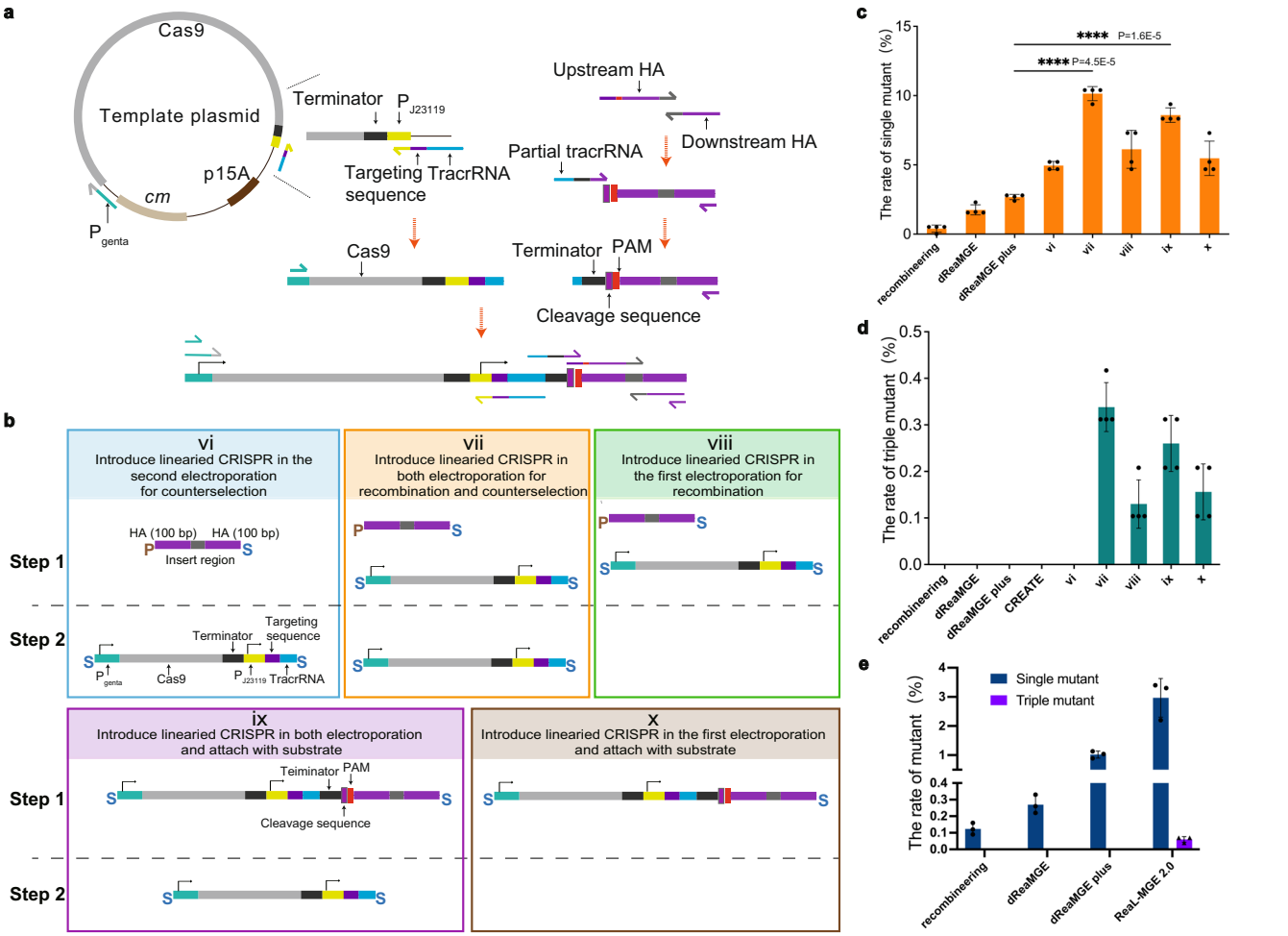

Fig. 4 | Establishment and utilization of ReaL-MGE 2.0 in *E. coli* BL21 and *S. brevitalea* DSM7029. a PCR strategy to assemble linear Cas9 and gRNA-expressing fragments with a targeting cassette as used in variations (vi) to (x). **b** Five protocol variations (vi – x) illustrate different combinations of linear dsDNA electroporated at steps 1 or 2. Cas9's expression is induced by arabinose in two recovery periods. **c** Single seamless mutagenesis efficiencies of *E. coli* mediated by (vi–x). **d** Triple seamless mutagenesis efficiencies of *E. coli* mediated by (vi) to (x) and other different dsDNA multiple demonstrations (dsDNA recombineering, dReaMGE, dReaMGE plus and CREATE). **e** Single/triple mutagenesis without selection in *S. brevitalea* DSM7029 utilizing recombineering, dReaMGE, dReaMGE plus, and ReaL-MGE 2.0. Values are means of the biological replicates, and the error bars indicate the standard deviations of all ($n = 4$ for **c**, **d**, and $n = 3$ for (**e**) biological replicates. *P*-values were obtained using the two-tailed Student's *t* test: $^{****}P < 0.0001$.

To screen for *E. coli* BL21 mutants with improved malonyl-CoA availability, we adapted a GFP reporter and growth-based sensor assay that had been developed in *S. cerevisiae*[67]. We codon optimized the FapR repressor for use in *E. coli* (Supplementary Data 1) and also varied the deployment of *fapO*, the FapR binding site, in the promoter of the *gfp*/*genta* operon (Supplementary Table 4) to optimize both repression in low intracellular malonyl-CoA concentration and the quantitative linkage between malonyl-CoA levels and the fluorescence intensity of GFP (Fig. 5a). The detection sensitivity of biosensor is enhanced by the codon-optimization of FapR repressor and rearrangement of *fapO* in the promoter region of *gfp*/*genta* operon, which effectively regulates the *gfp*/*genta* operon in response to varying concentrations of malonyl-CoA. Promoter J233, where two *fapO* are respectively placed behind the −35 region and −10 regions of promoter J23119 (Supplementary Fig. 5e), was selected for use in the malonyl-CoA sensor, which allows the inhibitory effect of 20 μg mL^{-1} gentamicin on mutants with intracellular malonyl-CoA titer lower than 0.1 nmol mg^{-1} DCW, while allowing for precise fluorescence output positively correlated to malonyl-CoA availability.

As illustrated in Fig. 5b, after one round of ReaL-MGE 1.0 aimed at the 28 targets, candidates were (a) required to express improved gentamicin resistance during the second recovery; (b) selected for elevated GFP expression by flow cytometry (Fig. 5c); (c) plated onto 20 μg mL^{-1} gentamicin plates to isolate single colonies; which were then (d) transferred to a microplate for (e) quantitation of the GFP signal. The best 150 candidates were then evaluated for intracellular malonyl-CoA (Fig. 5d), and clone 33# with the highest intracellular malonyl-CoA was named *E. coli* BL21.C33. *E. coli* BL21.C33 produced 1.165 nmol mg^{-1} DCW (Dry Cell Weight) of malonyl-CoA, which corresponds to a 26-fold increase compared with that of *E. coli* BL21 (0.045 nmol mg^{-1} DCW) (Fig. 5e).

Whole genome sequencing of *E. coli* BL21.C33 to a 500-fold genome coverage revealed 14 of the 28 targets were mutated simultaneously (10 genes, 3 transposons, and 1 prophage) and no unintended mutagenesis, either off-target effects or other genomic errors. In addition, *xseA* was also mutated as intended (Fig. 5f). The up-regulated genes were PGI (catalyzing the phosphorylation of glucose to glucose-6-phosphate, the first and rate-limiting step in glucose utilization), PAT (catalyzing the reversible transfer of an acetyl group from acetyl phosphate to CoA, yielding acetyl-CoA, a key step in various metabolic pathways), ACS (catalyzing the conversion of acetate into acetyl-CoA, a fundamental metabolic intermediate involved in numerous biochemical pathways), PPC (catalyzing the conversion of oxaloacetate into phosphoenolpyruvate), FBP (catalyzing the hydrolysis of fructose 1,6-

https://doi.org/10.1038/s41467-024-54191-4

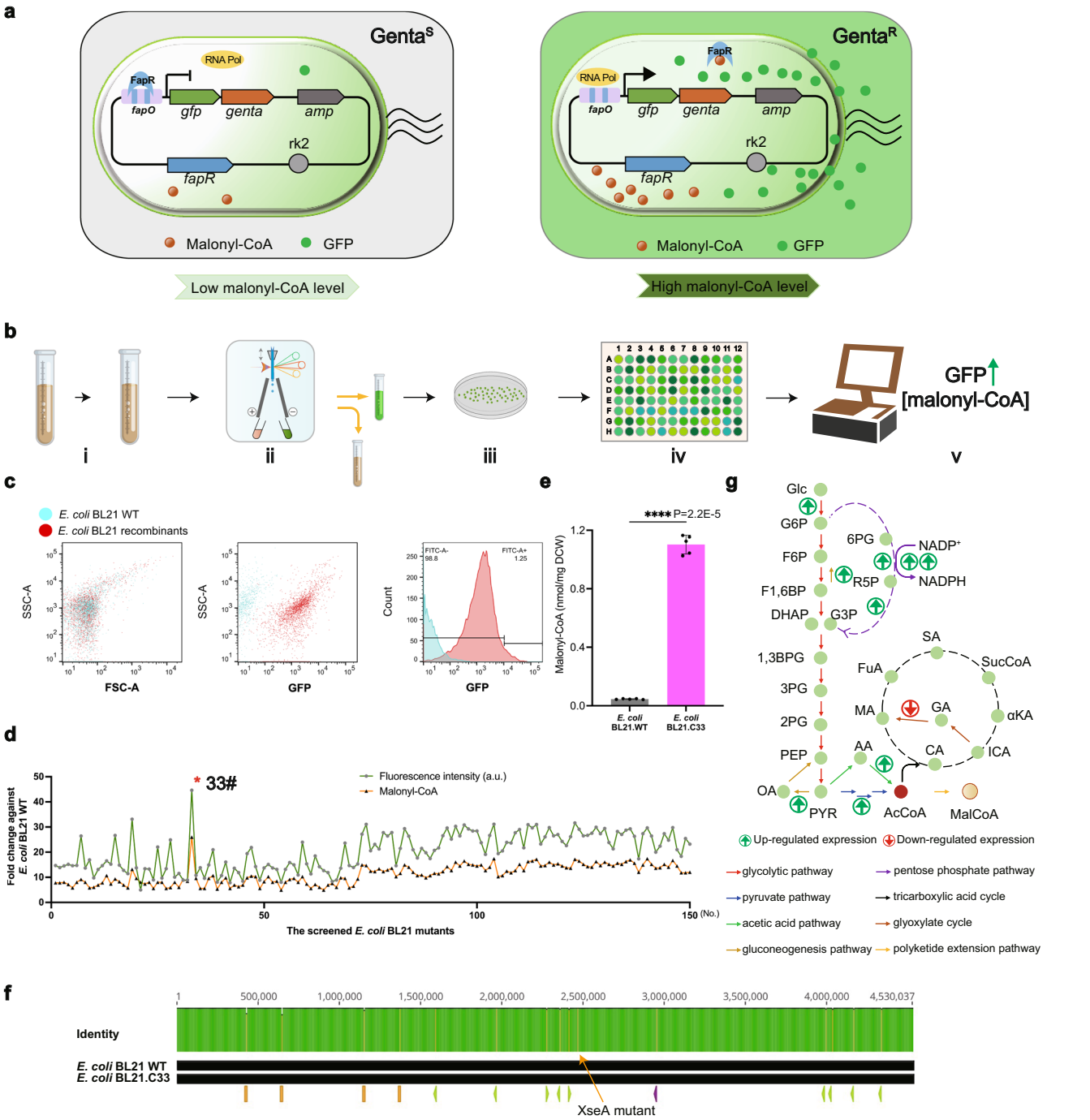

Fig. 5 | Application of ReaL-MGE 1.0 in the construction of *E. coli* BL21 malonyl-CoA chassis cells. a Scheme of the FapR biosensor. At low malonyl-CoA (left) the FapR repressor binds to *fapO* and prevents expression of the *gfp*/gentamicin resistance operon, rendering the host gentamicin sensitive. Elevated malonyl-CoA binds to FapR, inactivating its DNA binding to *fapO* and releasing expression of the *gfp*/gentamicin resistance operon. **b** Scheme of selection procedure to identify the elevated malonyl-CoA *E. coli* host. The second recovery in ReaL-MGE 1.0 (i) before FACS sorting for GFP expression (ii) and plating on gentamicin to isolate single colonies (iii) that were picked into microplates for GFP quantitation (iv) and HP-LC determination of intracellular malonyl-CoA concentration (v). **c** FACS analysis from step (ii) SSC - side scatter, FSC - forward scatter. **d** Intracellular malonyl-CoA concentrations were determined for 150 candidates, leading to the choice of clone 33# (*E. coli* BL21.C33) for further work. **e** Evaluation of malonyl-CoA in *E. coli* BL21 and the *E. coli* BL21.C33 derivative. **f** Whole genome sequencing of *E. coli* BL21.C33 showing mutated sites. Green arrows, malonyl-CoA metabolic pathway promoter replacements; purple arrow, LVA insertion; orange blocks, transposase/prophage deletions. The *xseA* gene was also mutated by the plasmid-borne inactivation cassette (Fig. 3a) as intended. **g** Schematic of the mutated metabolic genes in *E. coli* BL21.C33. Values are means of the biological replicates, and the error bars indicate the standard deviations of all ($n = 5$) biological replicates. *P*-values were obtained using the two-tailed Student's *t* test: ****$P < 0.0001$.

bisphosphate [F1,6BP] to fructose 6-phosphate [F6P]), GND (catalyzing the oxidative decarboxylation of gluconate-6-phosphate [G6P] to 6-phosphogluconolactone, concomitantly reducing $NADP^+$ to NADPH), TALA (generating ribose-5-phosphate [R5P] for nucleotide synthesis and NADPH for reductive biosynthetic reactions and oxidative stress defense), TPI (catalyzing the reversible isomerization of dihydroxyacetone phosphate [DHAP] into glyceraldehyde-3-phosphate [G3P], maintaining the flow of metabolites through the glycolytic pathway

https://doi.org/10.1038/s41467-024-54191-4

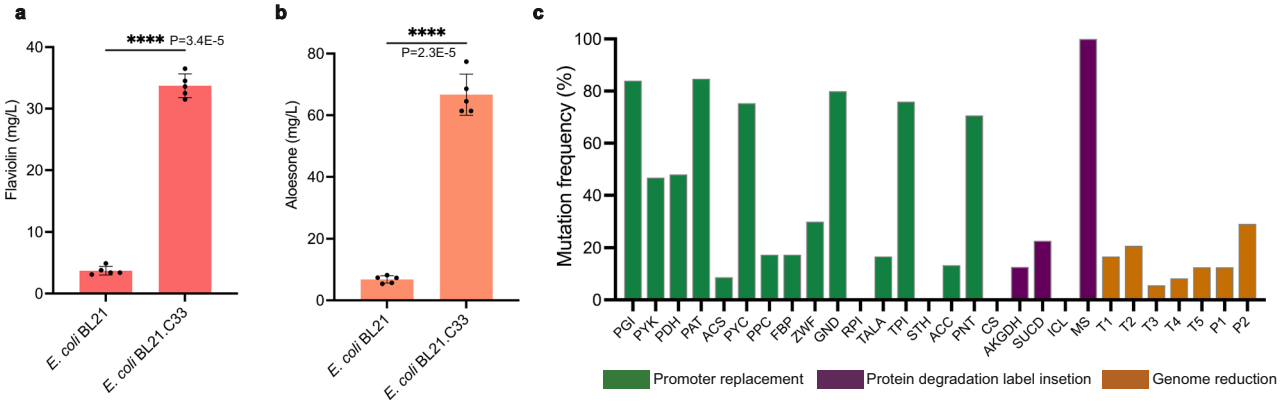

Fig. 6 | Functional performance in *E. coli* BL21 malonyl-CoA mutants. **a** Quantification of falviolin expression in *E. coli* BL21 and *E. coli* BL21.C33. **b** As (**a**) except aloesone expression. **c** Selection frequency of the 21 metabolic targets and 7 deletions in the 150 selected *E. coli* BL21 clones. Values are means of the biological replicates, and the error bars indicate the standard deviations of all ($n = 5$) biological replicates. *P*-values were obtained using the two-tailed Student's *t* test: $^{****}P < 0.0001$.

and for channeling intermediates into various metabolic pathways) and PNT (catalyzing the transfer of hydride ions [H^-] between the NADH and its phosphorylated counterpart, $NADP^+$, resulting in the generation of NADPH and NAD^+), while one down-regulated gene (that is, the LVA tag insertion) emerged, namely MS (catalyzing the formation of malate from acetyl-CoA and glyoxylate) (Fig. 5g and Supplementary Fig. 6). It's worth noting that, we have initially attempted to construct a gRNA co-expression plasmid targeting all 28 genes. Perhaps due to the instability of the plasmid caused by the presence of multiple repeat sequences, we were unable to obtain plasmids with more than 10 gRNA genes, which has also been reported previously[68]. This result proves the use of plasmids for multi-gRNA co-expression is time-consuming and inefficient.

Functional evaluation of ReaL-MGE in *E. coli* BL21

We utilized the expression of the RppA biosynthetic gene cluster (BGC) to evaluate the functional performance of *E. coli* BL21 candidates obtained in the last section. RppA is a type III polyketide synthase (PKS) that produces red-colored flaviolin. Sixty of the 150 candidates, including *E. coli* BL21.C33, and *E. coli* BL21 wild type strain (*E. coli* BL21 WT) were electroporated with an RppA expression plasmid. Flaviolin expression was strongly elevated over *E. coli* BL21 wild-type strain (*E. coli* BL21 WT) in all 60 with *E. coli* BL21.C33 amongst the strongest (Supplementary Fig. 7a). The yield of flaviolin reached 33.7 mg L^{-1} in *E. coli* BL21.C33, which is 9.1-fold of that in *E. coli* BL21 WT (3.7 mg L^{-1}) (Fig. 6a and Supplementary Fig. 7b). To further evaluate *E. coli* BL21.C33, we introduced a RpALS expression plasmid. RpALS is a type III PKS derived from *Rheum palmatum* that produces the direct aglycone precursor of Aloesin (aloesone)[35], which is a cosmetic raw material. Aloesone expression in *E. coli* BL21.C33 reached 77.4 mg L^{-1}, which was 11.4-fold higher than that in *E. coli* BL21 WT (6.8 mg L^{-1}) (Fig. 6b). The authenticity of flaviolin and aloesone produced by *E. coli* BL21.C33 was confirmed by LC-MS and MS/MS analysis (Supplementary Fig. 7c, d). The 48 h growth curve and viable count of *E. coli* BL21.C33 and *E. coli* BL21 WT showed that the growth state of *E. coli* BL21.C33 is modestly improved (Supplementary Fig. 8a, b). The production of flaviolin and aloesone in different candidates was also examined, and the results showed that the increase of these malonyl-CoA derivatives was dependent on the increase of malonyl-CoA levels (Supplementary Fig. 8c).

Based on these affirmations that malonyl-CoA levels were elevated by ReaL-MGE, we inspected the mutational profile of the 150 candidates for the mutagenic frequencies of the 28 targets (Fig. 6c). Seven genes (MS, PAT, PGI, GND, TPI, PYC, PNT) were frequently mutated (> 50%), suggesting that these genes may be critical factors in malonyl-CoA accumulation of *E. coli* BL21. Previous studies reported that manipulating the expression levels of PGI, GND, TPI, PNT, and MS genes elevated intracellular malonyl-CoA levels[69,70]. Mutagenesis of PYC is notable. Although previously associated with elevated malonyl-CoA titers, mutagenesis of PYC was also accompanied by impaired cell growth[39]. We reason that the high frequency of selected PYC mutagenesis in our multiplex strategy has been accompanied by unexpected compensation(s) for the cell growth impairment.

Another notable observation involves the high selection frequency (80%) of PAT (phosphate acetyltransferase) elevated expression. Individual enhancement of PAT expression only slightly increased malonyl-CoA levels (Supplementary Fig. 5d). We conducted a comprehensive analysis of the individual editing efficiencies across all 21 selected target sites, which revealed that mutagenesis differed by less than two-fold overall (Supplementary Fig. 7e). Therefore, the high selection frequency of PAT was not due to preferential mutagenesis. Conversely, STH was most efficiently mutagenized, however not selected amongst the 150 mutant strains at all (Fig. 6c). This discrepancy suggests that the selection of these 150 mutants was primarily driven by the intracellular malonyl-CoA titer rather than the ease of mutagenesis. The high frequency (80%) selection of PAT overexpression and low frequency (0%) selection of STH overexpression amongst the selected mutants further supports the proposition that the prokaryotic metabolic network includes complex linkages currently beyond rationale and multiplex approaches are required to uncover these complexities.

Application of ReaL-MGE for elevated malonyl-CoA in *S. brevitalea* DSM7029

To apply ReaL-MGE 2.0 in *S. brevitalea* DSM7029, we focused on the same 21 enzymes involved in nine malonyl-CoA synthetic or competing pathways and added another gene (SBM), which is not present in *E. coli* BL21. These enzymes were also targeted by the two strategies: (i) insertion of the P_{genta} promoter and gentamicin resistance gene to enhance their expression (765 bp) and (ii) incorporation of the LVA protein degradation tag along with the gentamicin resistance gene to attenuate protein expression (795 bp). Glidobactin NRPS-PKS hybrid compound produced by glb BGC of *S. brevitalea* DSM7029 exhibits a unique absorption signature at 254 nm, allowing preliminary assess the intracellular malonyl-CoA concentration of the mutants (Fig. 7a). A total of 192 mutants were selected from the plate containing an elevated concentration of gentamicin (30 μg mL^{-1}) for the purpose of measuring the absorption peak at 254 nm. Upon examination, it was discovered that 103 mutants exhibited a significant alteration in the 254 nm absorption peak compared to the *S. brevitalea* DSM7029 wild-

https://doi.org/10.1038/s41467-024-54191-4

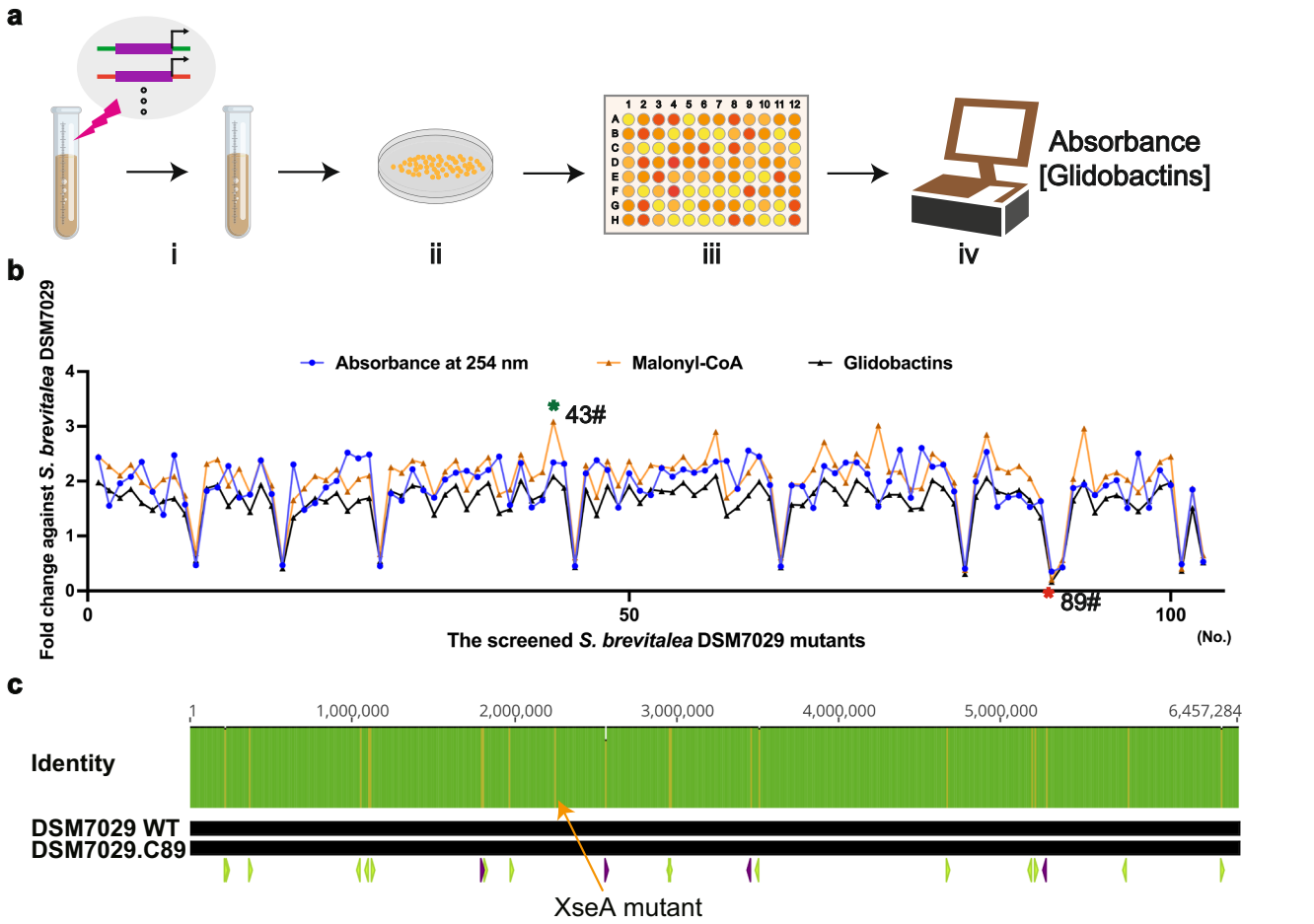

Fig. 7 | Validation of the ability of ReaL-MGE 2.0 to mediate simultaneous editing of multiple kilobase-scale sequences in *S. brevitalea* DSM7029. a Flow chart of the screening of *S. brevitalea* DSM7029 mutants with modified malonyl-CoA metabolic network by glidobactin yield. Using ReaL-MGE 2.0 to mediate 22 kilobase-scale sequence insertion in *S. brevitalea* DSM7029 (i), the bacterial solution was spread on the plate containing an elevated concentration of gentamicin (30 μg mL^{-1}) (i). Colonies were selected from plates and inoculated into 96-well plates for culture (iii). The 254 nm absorption intensity of the selected mutants was detected (iv). **b** Absorbance at 254 nm, intracellular malonyl-CoA concentrations, and glidobactins' yield determined for 103 selected mutants leading to the choice of clones 43# (*S. brevitalea* DSM7029.C43) and 89# (*S. brevitalea* DSM7029.C89) for further detection. **c** Whole genome sequencing of *S. brevitalea* DSM7029.C89 showing mutated sites. Green arrows, malonyl-CoA metabolic pathway promoter replacements; purple arrows, LVA insertion.

type strain (*S. brevitalea* DSM7029 WT). Of these, 93 mutants displayed a peak value exceeding 1.5-fold the level of the wild type, whereas 10 mutants showed a peak value below 0.5-fold that of the *S. brevitalea* DSM7029 WT. We further assayed the intracellular malonyl-CoA titer and glidobactin yield of these 103 mutants and observed a consistent trend among the 254 nm absorption peak, malonyl-CoA concentration and glidobactin yield (Fig. 7b). The mutant *S. brevitalea* DSM7029.C89, exhibiting the lowest intracellular malonyl-CoA titer, was confirmed through PCR analysis to possess the anticipated edits at 21 target sites. Furthermore, whole-genome sequencing revealed the successful insertion of 21 kilobase-scale sequences into the *S. brevitalea* DSM7029 genome, without any evidence of off-target effects in *S. brevitalea* DSM7029.C89 (Fig. 7c and Supplementary Fig. 9). This result not only underscores the proficiency of ReaL-MGE in editing multiple large fragments but also further proves that the multi-layered networks are difficult to unpredict, the genotype diversity caused by the unsaturation of editing efficiency of ReaL-MGE is more conducive to the acquisition of ideal mutants.

Given the importance of editing efficiency and the demand for high-throughput screening, we adopted an approach similar to that used in *E. coli* BL21 to construct and screen *S. brevitalea* DSM7029 malonyl-CoA chassis cells. Previously we showed that deletion of deleterious genomic regions in *S. brevitalea* DSM7029 enhanced the heterologous production of NRP/PKS products[46,61]. To engineer *S. brevitalea* DSM7029 for enhanced malonyl-CoA expression, we coupled the deletion of 9 deleterious genomic regions (spanning a total of 300 kb; Supplementary Table 5) with promoter replacement (166 bp) or addition of the LVA protein degradation tag (30 bp) targeting the 22 rate-limiting enzymes. The genome of *S. brevitalea* DSM7029 contains 17 predicted BGCs but only glidobactin and glidomide BGCs are active under laboratory growth. Because glidobactin NRP-PKS hybrid synthesis could interfere with the quantitative analysis of malonyl-CoA, a glidobactin BGC deletion strain, *S. brevitalea* DSM7029Δglb, was used as the host for ReaL-MGE 2.0.

The RK2-P_{fapO}-GFP-genta-fapR$_{7029}$ screening system was employed (Fig. 8a) to select 150 colonies for malonyl-CoA analysis (Fig. 8b) and clone 21# (*S. brevitalea* DSM7029Δglb.C21) was selected as the leading candidate. Whole genome sequencing to 500-fold genome coverage revealed the simultaneous modification of 17 genomic regions, including 11 promoter replacements, 2 LVA insertions, and 3 genomic deletions (of 90 kb in total), as well as the *xseA* knock-out, with no off-target errors (Fig. 8c and Supplementary Fig. 10). Malonyl-CoA levels in *S. brevitalea* DSM7029Δglb.C21 were elevated 20-fold over *S. brevitalea* DSM7029Δglb (0.045 to 0.92 nmol mg^{-1} DCW) (Fig. 8d). Genotype analysis of the 150 mutants (Fig. 8e) identified several up- and down-regulated expression genes, including

https://doi.org/10.1038/s41467-024-54191-4

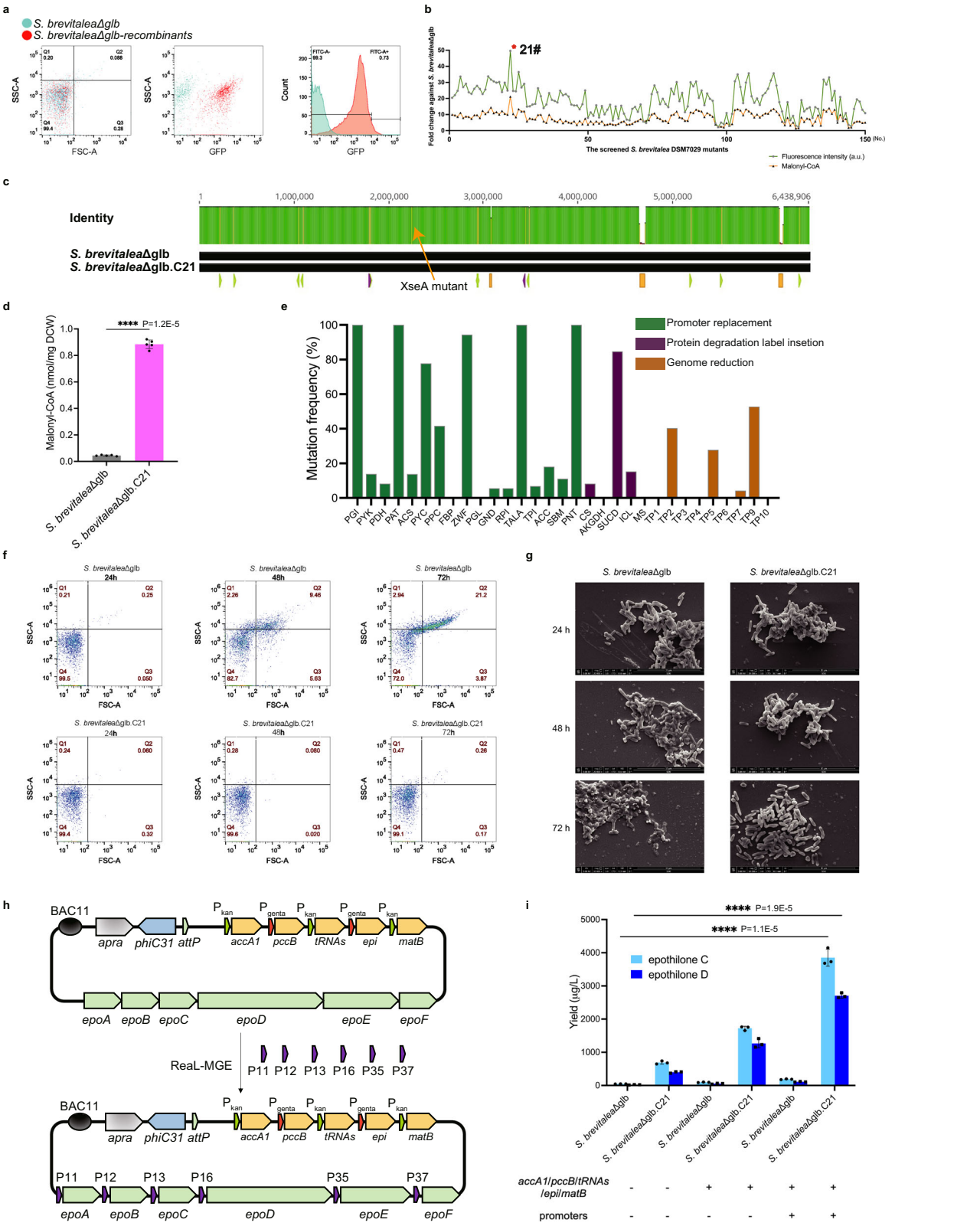

PGI, PAT, PYC, glucose-6-phosphate dehydrogenase (ZWF), TALA, PNT and SUCD (> 50%), suggesting that these genes maybe critical factors in malonyl-CoA accumulation of *S. brevitalea* DSM7029. Notably, growth of *S. brevitalea* DSM7029Δglb.C21 was improved compared to *S. brevitalea* DSM7029 and *S. brevitalea* DSM7029Δglb (Supplementary Fig. 11). As we previously described, cell death associated with proliferation hindered the potential of *S. brevitalea* DSM7029 as a cell factory. Flow cytometry analysis of *S. brevitalea* DSM7029Δglb and *S. brevitalea* DSM7029Δglb.C21 after 24, 48, and 72 h culture showed that DSM7029Δglb was also impacted by cell death whereas DSM7029Δglb.C21 continued in robust growth after 72 hours of culture (Fig. 8f). In addition, a comparison of cell morphologies at 24, 48, and 72 h using FESEM revealed that *S. brevitalea* DSM7029Δglb exhibited cell autolysis as early as 24 hours, whereas *S. brevitalea*

Fig. 8 | Application of ReaL-MGE 2.0 in the construction of *S. brevitalea* DSM7029 malonyl-CoA chassis cells. a FACS sorting for GFP expression from the FapR biosensor. SSC - side scatter, FSC - forward scatter. **b** Intracellular malonyl-CoA concentrations were determined for 150 candidates leading to the choice of clone 21# (*S. brevitalea* DSM7029Δglb.C21) for further work. **c** Whole genome sequencing of *S. brevitalea* DSM7029Δglb.C21 showing mutated sites. Green arrows, malonyl-CoA metabolic pathway promoter replacements; purple arrows, LVA insertion; orange blocks, transposase/prophage deletions. **d** Evaluation of malonyl-CoA in *S. brevitalea* DSM7029Δglb and *S. brevitalea* DSM7029Δglb.C21. **e** Selection frequency of the 22 metabolic targets and 9 deletions in the 150 selected *S. brevitalea* DSM7029Δglb clones. **f** FACS analysis using side and forward scatter during growth of *S. brevitalea* DSM7029Δglb and *S. brevitalea* DSM7029Δglb.C21 to evaluate cell death at 24, 48, and 72 h in batch culture. **g** Images of cells from the growth experiment of (**f**). The experiment was repeated twice independently with similar results. **h** Scheme of ReaL-MGE 1.0 to replace the promoters of the *epoA-epoF* BGC with artificial promoters. P11, P12, P13, P16, P35 and P37 are described in previous study[72]. **i** Quantitation of epothilone C/D yields obtained from *S. brevitalea* DSM7029Δglb and *S. brevitalea* DSM7029Δglb.C21 using the epo BGC BAC with or without the *accA1/pccB/tRNA/epi/matB* cassette and/or the six-promoter exchange as indicated. Values are means of the biological replicates, and the error bars indicate the standard deviations of all ($n = 5$ for **d** and $n = 3$ for **i**) biological replicates. *P*-values were obtained using the two-tailed Student's *t* test: ****$P < 0.0001$.

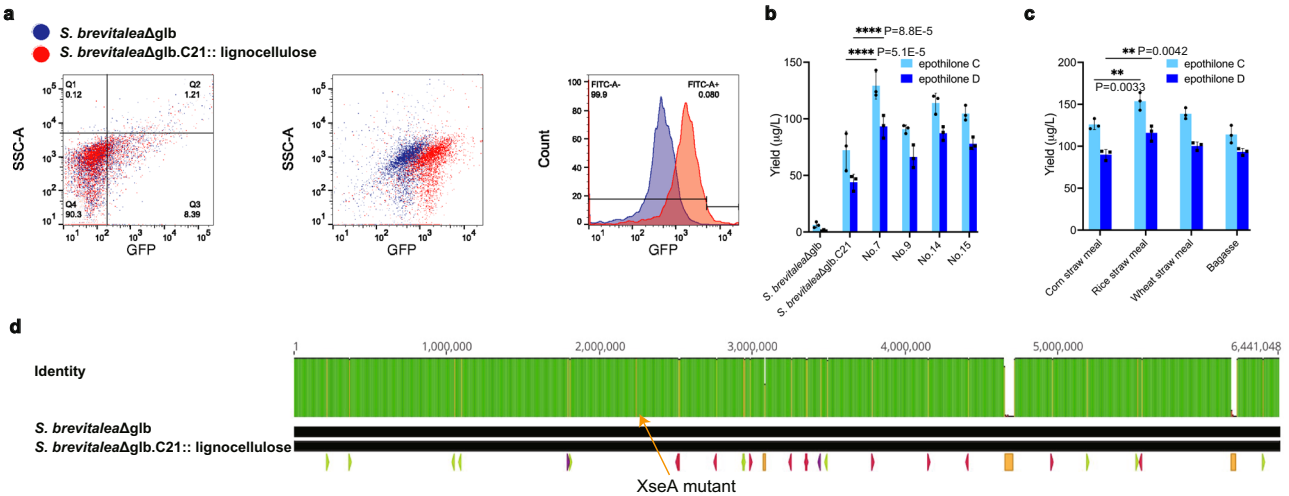

Fig. 9 | The ReaL-MGE 2.0 mediated construction of *S. brevitalea* DSM7029Δglb.C21:: lignocellulase. a The FCM results showing FSC data plotted against SSC and FITC data against SSC of the *S. brevitalea* DSM7029Δglb.C21 and *S. brevitalea* DSM7029Δglb.C21 mutants with activation of lignocellulases. **b** The yield of epothilone C/D in *S. brevitalea* DSM7029Δglb, *S. brevitalea* DSM7029Δglb.C21, and mutants with activation of lignocellulases using corn straw meal as only carbon source. The yield of epothilone C/D in the No.7 mutant using corn straw meal as the only carbon source was increased by 1.8/2.1-fold compared with that in *S. brevitalea* DSM7029Δglb.C21. **c** The yield of epothilone C/D in the No.7 mutant using different natural lignocellulose as only carbon source. **d** Comparison of genome sequence of *S. brevitalea* DSM7029Δglb.C21:: lignocellulose and *S. brevitalea* DSM7029Δglb. Green arrows, malonyl-CoA metabolic pathway promoter replacements; purple arrows, LVA insertion; orange blocks, transposase/prophage deletions; pink arrows, lignocellulase promoter replacement. Values are means of the biological replicates, and the error bars indicate the standard deviations of all ($n = 3$) biological replicates. *P*-values were obtained using the two-tailed Student's *t* test: **$P < 0.01$, ****$P < 0.0001$.

DSM7029Δglb.C21 maintained intact cell shapes without detectable lysis even after 72 h of cultivation (Fig. 8g). These results further confirm that *S. brevitalea* DSM7029Δglb.C21 is a promising platform strain for comprehensive optimization of both growth and production.

To evaluate our progress, we assessed the capacity of *S. brevitalea* DSM7029Δglb.C21 to synthesize epothilone, which is an NRPS-PKS hybrid anticancer compound that stabilizes microtubules and exhibits efficacy against taxane-resistant cells with promising clinical potential for advanced breast cancer therapy[37]. We enhanced the epothilone BGC (epo BGC) by the addition of a cassette containing four key genes (propionyl-CoA carboxylase [*accA1-pccB*], methylmalonyl-CoA epimerase [*epi*], malonyl-CoA synthetase [*matB*], and also rare tRNA genes)[61,71,72]. We also used two rounds of ReaL-MGE 1.0 in *E. coli* to replace promoters of the six core genes (*epoA-epoF*) (Fig. 8h). The three different versions of the epo BGC were integrated into the genomes of *S. brevitalea* DSM7029Δglb and *S. brevitalea* DSM7029Δglb.C21 using *attP* transposase and epothilone yield evaluated by LC-MS and MS/MS analysis, the highest epothilone C/D levels were (4.1/2.7 mg L^{-1}) elevated by 89/128-fold compared to the unmodified epo BGC BAC in DSM7029Δglb (46/21 μg L^{-1}) (Fig. 8i and Supplementary Fig. 12a, b). We also rigorously verified that the elevated production of epothilones in various *S. brevitalea* mutants directly correlates with increased levels of malonyl-CoA (Supplementary Fig. 12c).

Adaptation of malonyl-CoA elevation to a lignocellulose carbon source

Lignocellulose is an abundant renewable resource that could add value to the development of bacterial cell factories. Genome sequencing analysis of *S. brevitalea* DSM7029 revealed the presence of lignocellulases, including eight cellulases, four hemicellulases, and six ligninases, indicating a potential to utilize lignocellulose (Supplementary Table 6). However, transcriptome data indicated that most lignocellulases were expressed at low levels under laboratory conditions. To activate the lignocellulose metabolism network and confirm the genome stability of the chassis created by ReaL-MGE, we performed a second round of ReaL-MGE 2.0 in *S. brevitalea* DSM7029Δglb.C21 aimed at 18 lignocellulases. To screen for strains that could utilize lignocellulose straw powder (specifically, corn stalk meal) as the sole carbon source, we used a malonyl-CoA biosensor (RK2-P_{fapO}-GFP-genta-fapR$_{7029}$) and flow cytometry (Fig. 9a) to select 30 candidates (Supplementary Fig. 13a, b). Subsequently, four mutants exhibiting higher malonyl-CoA concentrations (No.7, No.9, No.14, and No.15) were selected to assess the production capability of epothilone C/D using corn straw meal as the sole carbon source and No.7 demonstrated the highest efficiency (Fig. 9b). Moreover, No.7 also displayed the ability to utilize rice straw meal, wheat straw meal, and bagasse as the sole carbon sources with rice straw meal delivering an epothilone C/D yield of 124.3 μg g^{-1} (Fig. 9c). Genome sequencing of

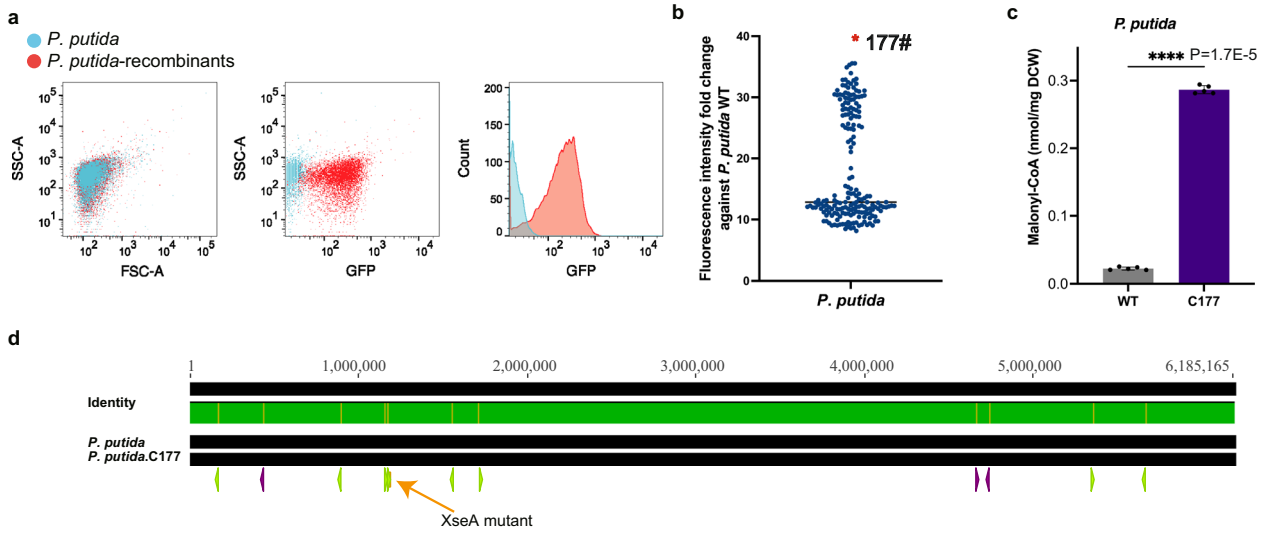

Fig. 10 | Application of ReaL-MGE 1.0 to improve intracellular malonyl-CoA titer of *P. putida*. **a** FACS sorting for GFP expression from the FapR biosensor in *P. putida* wild type and recombinants. **b** Fluorescence intensity was determined for 192 candidates leading to the choice of clone 177# (*P. putida*.C177) for further work in *P. putida*. **c** Evaluation of malonyl-CoA in *P. putida* wild type and *P. putida*.C177. **d** Comparison of genome sequence of *P. putida*.C177 and *P. putida* wild type. Green arrows, malonyl-CoA metabolic pathway promoter replacements; purple arrows, LVA insertion. Values are means of the biological replicates, and the error bars indicate the standard deviations of all ($n = 5$) biological replicates. *P* values were obtained using the two-tailed Student's *t* test: $^{****}P < 0.0001$.

No.7 revealed promoter replacement of 12 lignocellulases, including four cellulases (catalyzing the hydrolysis of cellulose into smaller oligosaccharides and ultimately glucose units): endocellulase (AAW51_2245), cellulose 1,4-β-cellobiosidase (AAW51_2246), β-glucosidases (AAW51_3720, AAW51_4231); three hemicellulases (catalyzing hemicellulose into smaller oligosaccharides and monosaccharides): mannan endo-1,4-β-mannosidase B (AAW51_2458), endo-1,4-β-xylanase (AAW51_2810), xylose-responsive-transcription regulator (AAW51_3235); and five ligninases (catalyzing the oxidative cleavage of the various chemical bonds present in lignin, leading to its depolymerization into smaller fragments and eventually to the release of constituent aromatic compounds): arylesterase (AAW51_2902), laccase (AAW51_2906), Mn-containing catalase (AAW51_2669), peroxidase (AAW51_3495), and CMC-oxidoreductase (AAW51_4754) (Fig. 9d and Supplementary Fig. 13c). No.7 was hence designated as *S. brevitalea* DSM7029Δglb.C21:: lignocellulase. Genome sequencing also confirmed the absence of off-target effects (Fig. 9d). After two rounds of ReaL-MGE 2.0 mediated engineering, a total of 29 genome regions of *S. brevitalea* DSM7029Δglb.C21:: lignocellulase were manipulated without causing any off-target effects, demonstrating the efficacy, stability and accuracy of ReaL-MGE, as well as its significant advantages over other CRISPR/Cas-assisted multiplex genome engineering technologies.

Application of ReaL-MGE for elevated malonyl-CoA in *Pseudomonas putida*

To enhance confidence that ReaL-MGE can be applied to further bacterial hosts, we engineered the malonyl-CoA metabolic network of *P. putida* KT2440. Using ReaL-MGE 1.0, we simultaneously targeted 21 genes (Supplementary Table 3), and then utilized a fapO-fapR-GFP biosensor (RK2-P_{fapO}-GFP-genta-$FapR_{kt2440}$) to identify mutants with increased fluorescence intensity, indicative of enhanced metabolic activity (Fig. 10a). The mutant *P. putida*.C177 exhibited a 35-fold increase in fluorescence intensity, suggesting a significant metabolic shift (Fig. 10b). Genetic analysis confirmed that 11 of the 21 genes were co-edited in this high-performing mutant (Supplementary Fig. 14a, b) and malonyl-CoA quantitation showed a 13.5-fold increase compared to the *P. putida* KT2440 wild type strain (0.0226 to 0.2866 nmol mg^{-1} DCW) (Fig. 10c). Whole genome sequencing to 500-fold genome coverage revealed the simultaneous modification of 12 genomic regions, including 8 promoter replacements and 3 LVA insertions, as well as the *xseA* knock-out, with no off-target errors (Supplementary Table 7) (Fig. 10d and Supplementary Fig. 14c, 14d).

The successful application of ReaL-MGE in *P. putida* underscores its universality and highlights the feasibility of utilization in multiplex genome engineering of procaryotic cells. The consistent increase in malonyl-CoA levels across different bacteria not only demonstrates the effectiveness of the ReaL-MGE technology but also suggests a universal metabolic engineering strategy that can be applied across different species. This applicability of ReaL-MGE, from *E. coli* to *S. brevitalea* and *P. putida*, broadens the scope of synthetic biology, enabling more complex and efficient genetic engineering endeavors.

Discussion

The complexities of microbial secondary metabolism challenge both its potential for medicine and commerce and the frontiers of organic chemistry. Unraveling these complexities has been unexpectedly difficult. In the absence of the understanding required for the ability to design solutions, new technical capacities are required. Multiplex mutagenesis combined with powerful selection strategies has the potential to solve these quandaries and elucidate mutagenic combinations relevant to the exploitation of microbial factories.

Here we expanded multiplex mutagenesis by enhancing the use of dsDNAs. We report the development of a ReaL-MGE, which harmonizes the RNA-guided programmability of CRISPR with the 5′-3′ exonuclease and SSAP activities of phage recombinases. A key advance enabling ReaL-MGE was the manipulation of ExoVII by mutating *xseA* and overexpressing *xseB*. This strategy enhanced recombineering in all three hosts tested and is recommended for recombineering in other bacteria. Multiplex dsDNA mutagenic strategies embrace several advantages, including (i) the ability to incorporate long segments that can encode added functions, such as an antibiotic or fluorescent selectable genes, gene regulatory regions, or the introduction of additional enzymes; (ii) the ability to simultaneously insert these long segments into multiple distance genomic loci; (iii) utilization of PCR to generate the dsDNA, which brings flexible design advantages including the positioning of the two homology arms to insert or delete at a broad spectrum of genomic target sites; (iv) PCR automation to generate

multiple candidate genomic targets to multiplex the genome for subsequent selection; and (v) bypass of the challenges associated with co-expression of multiple gRNAs from plasmid(s). We compare ReaL-MGE with existing multiplex strategies and confirm that ReaL-MGE significantly extends the multiplex repertoire beyond the use of ss-oligonucleotides and plasmids (Supplementary Table 7). ReaL-MGE 1.0 is applicable to bacterial strains adept at managing the cytotoxic effects inherent in the CRISPR/Cas9 system, which includes well-established model organisms like *E. coli* and *P. putida*. ReaL-MGE 2.0 utilizes a linearized CRISPR/Cas9 system to modulate toxicity in bacteria with limited tolerance to CRISPR/Cas9, such as *S. brevitalea* DSM7029.

The unexpected complexity of the challenges posed by microbial metabolic engineering can be seen in the variety of results we obtained whilst enhancing malonyl-CoA expression in different bacteria. To consider these results, in Supplementary Table 7, we analyzed mutations identified in the three best-elevated malonyl-CoA strains (*E. coli* BL21.C33, *S. brevitalea* DSM7029Δglb.C21 and *P. putida*.C177), and found only five (PGI, PAT, ACS, TALA, PNT) of the 21 target genes have all been edited in these three mutations. These five genes act as universal key genes of the malonyl-CoA metabolic network, suggesting that enhancing glucose utilization, promoting acetyl-CoA synthesis, and increasing NADPH supply are general strategies to increase the intracellular malonyl-CoA concentration in bacteria. Notwithstanding the common observation of these 5 genes, little concordance emerged from the multiplex mutagenesis screens, which is an indication of network complexity and outlines the problems involved with understanding microbial secondary metabolism (Supplementary Table 7). Possibly, information gathered from multiplex mutagenesis using both ss-oligo and now dsDNA approaches using ReaL-MGE can provide insights for future design, and there is no doubt that multiplex network mapping will be needed whenever a metabolic challenge in a new host is embraced.

Despite numerous studies focused on enhancing intracellular malonyl-CoA levels[57,73], the identification of genetic targets and mutagenic combinations has been impeded not only by the intricate metabolic networks but also by impaired growth due to metabolic perturbations. We utilized ReaL-MGE to combine mutants aimed at elevated malonyl-CoA expression with genomic region deletions aimed at growth maintenance. Thereby, we generated *E. coli* and *S. brevitalea* strains that can be used as platforms for further applications of PKS and PAS secondary metabolite engineering. Through measurements of malonyl-CoA yield at various fermentation time points, coupled with sequencing the targeted sites post-fermentation, we conclude that the engineered strains exhibit reliable production capacity and genetic stability. Therefore, we suggest that ReaL-MGE is a reliable and efficient method for strain engineering, resulting in robust and genetically stable strains for malonyl-CoA production (Supplementary Fig. 15).

While ReaL-MGE has been successfully implemented in some prokaryotic species, the feasibility of using it for gene engineering in eukaryotic cells still presents several challenges. In eukaryotic species especially in mammalian cells, the genomes are typically larger and more complex, which complicates efficient editing. Furthermore, delivering large PCR fragments into eukaryotic cells is more difficult due to differences in cell structure and uptake mechanisms. Another significant hurdle is that eukaryotic cells predominantly use non-homologous end joining (NHEJ) for DNA repair and lack universal efficient homologous recombinases, which can reduce the efficiency and accuracy of homologous recombination-based editing systems like ReaL-MGE. To overcome these challenges, several strategies could be employed. Developing efficient viral or non-viral delivery systems specifically tailored for eukaryotic cells could enhance the uptake of ReaL-MGE components. Modifying eukaryotic cells and mining efficient homolog recombinase to favor homologous recombination over NHEJ to improve accurate editing efficiency. While more adaptations are required, the foundational principles of ReaL-MGE provide a promising starting point for future advancements in eukaryotic genome editing.

Furthermore, we demonstrated that dsDNA multiplex mutagenesis can be used for the prioritization of growth concomitantly with the extension of metabolic flexibility. Our dsDNA multiplex logic is likely to yield similar successes when applied to other metabolic engineering challenges.

Methods

Strains, plasmids, and mutants

All bacteria strains, plasmids, and mutants are described in Supplementary Data 2.

Plasmid construction

Oligonucleotides were synthesized from Tsingke Biological Technology and Sangon Biotech, and are described in Supplementary Data 2. *cas9*, *enAsCas12a*, *AsCas12f1*, *fapRecoli*, *fapR7029*, *accA*, *pccB*, *tRNA*, *matB,* and *epi* were synthesized from Beijing Genomics institution (BGI) in Supplementary Data 1.

pBBR1-P_{Rha}-Redγβα-P_{BAD}-Cas9-Km. This expression plasmid is based on a pBBR1 origin and harbors the recombinase genes under the control of the Rha promoter and the *cas9* gene under the control of the BAD promoter. For the initial construct, the original pBBR1-P_{Rha}-Redγβα-Km and the amp-ccdB cassette amplified from R6K-amp-ccdB with primers gba-amp-ccdB-1/gba-amp-ccdB-2 were co-transformed into GB05-red-gyrA462 induced for the expression of Redα/Redβ and selected on LB plates containing 100 μg mL^{-1} ampicillin (37 °C) for linear plus circle homologous recombination (LCHR) to assemble pBBR1-P_{Rha}-Redγβα-Km-amp-ccdB[74]. The pBBR1-P_{Rha}-Redγβα-Km-amp-ccdB was digested (SacI) to linear fragment and co-transformed with BAD-Cas9 cassette amplified from RK2-P_{BAD}-Cas9-genta with primers BAD-Cas9-1/BAD-Cas9-2 into GB05-dir induced for the expression of full-length RecE/RecT and selected on LB plates containing 15 μg mL^{-1} kanamycin (37 °C) for linear plus linear homologous recombination (LLHR) to assemble pBBR1-P_{Rha}-Redγβα-P_{BAD}-Cas9-Km by LLHR[75,76].

pBBR1-P_{Rha}-Redγβα-xseB-Km. This plasmid was added *xseB* gene from *E. coli* to pBBR1-P_{Rha}-Redγβα-Km. The linear fragment digested (SacI) from pBBR1-P_{Rha}-Redγβα-Km-amp-ccdB and *xseB* gene amplified from *E. coli* with primers xseB-ecoli-1/xseB-ecoli-2 were co-transformed into GB05-dir and selected on LB plates containing 15 μg mL^{-1} kanamycin (37 °C) to assemble pBBR1-P_{Rha}-Redγβα-xseB-Km by LLHR.

pBBR1-P_{Rha}-Redγβα-xseB-P_{BAD}-Cas9-Km. This plasmid was added *xseB* gene from *E. coli* to pBBR1-P_{Rha}-Redγβα-P_{BAD}-Cas9-Km. The linear fragment digested (SacI) from pBBR1-P_{Rha}-Redγβα-Km-amp-ccdB, *xseB* gene amplified from *E. coli* with primers xseB-ecoli-1/xseB-ecoli-2 and BAD-Cas9 cassette were co-transformed into GB05-dir and selected on LB plates containing 15 μg mL^{-1} kanamycin (37 °C) to assemble pBBR1-P_{Rha}-Redγβα-xseB-P_{BAD}-Cas9-Km by LLHR.

pBBR1-P_{Rha}-Redγβα-xseB-P_{BAD}-Cas9-xseAi-Km. This plasmid was added xseAi for *E. coli* to pBBR1-P_{Rha}-Redγβα-xseB-P_{BAD}-Cas9-Km. The linear fragment digested (SacI) from pBBR1-P_{Rha}-Redγβα-Km-amp-ccdB, *xseB* gene, xseAi cassette synthesized from BGI and BAD-Cas9 cassette was co-transformed into GB05-dir and selected on LB plates containing 15 μg mL^{-1} kanamycin (37 °C) to assemble pBBR1-P_{Rha}-Redγβα-xseB-P_{BAD}-Cas9-xseAi-Km by LLHR.

pBBR1-P_{Rha}-Redγ-Redαβ7029-xseB7029-Km. The original pBBR1-P_{Rha}-Redγ-Redαβ7029-Km and the amp-ccdB cassette amplified from R6K-amp-ccdB with primers g6457-amp-ccdB-1/g6457-amp-ccdB-2 were co-transformed into GB05-red-gyrA462 and selected on LB plates containing 100 μg mL^{-1} ampicillin (37 °C) to assemble pBBR1-P_{Rha}-Redγ-Redαβ7029-Km-amp-ccdB by LCHR. The pBBR1-P_{Rha}-Redγ-Redαβ7029-Km-amp-ccdB was digested (SacI) to linear fragment and co-transformed with *xseB* gene amplified from *S. brevitalea* DSM7029 with primers xseB-7029-1/xseB-7029-2 into GB05-dir and selected on LB plates containing 15 μg mL^{-1} kanamycin (37 °C) to assemble pBBR1-P_{Rha}-Redγ-Redαβ7029-xseB7029-Km by LLHR.

pBBR1-P_{Rha}-BAS-xseBkt2440-Km. The original pBBR1-P_{Rha}-BAS-Km and the amp-ccdB cassette amplified from R6K-amp-ccdB with primers BAS-amp-ccdB-1/BAS-amp-ccdB-2 were co-transformed into GB05-red-gyrA462 and selected on LB plates containing 100 μg mL^{-1} ampicillin (37 °C) to assemble pBBR1-P_{Rha}-BAS-Km-amp-ccdB by LCHR. The pBBR1-P_{Rha}-BAS-Km-amp-ccdB was digested (SacI) to linear fragment and co-transformed with *xseB* gene amplified from *P. putida* KT2440 with primers xseB-kt2440-1/xseB-kt2440-2 into GB05-dir and selected on LB plates containing 15 μg mL^{-1} kanamycin (37 °C) to assemble pBBR1-P_{Rha}-BAS-xseBkt2440-Km by LLHR.

pBBR1-P_{Rha}-BAS-xseBkt2440-P_{BAD}-Cas9-Km. This plasmid was added *xseB* gene from *P. putida* to pBBR1-P_{Rha}-BAS-P_{BAD}-Cas9-Km. The linear fragment digested (SacI) from pBBR1-P_{Rha}-BAS-Km-amp-ccdB, *xseB* gene amplified from *P. putida* with primers xseB-kt2440-1/xseB-kt2440-2 and BAD-Cas9 cassette were co-transformed into GB05-dir and selected on LB plates containing 15 μg mL^{-1} kanamycin (37 °C) to assemble pBBR1-P_{Rha}-BAS-xseBkt2440-P_{BAD}-Cas9-Km by LLHR.

pBBR1-P_{Rha}-BAS-xseBkt2440-P_{BAD}-Cas9-xseAi-Km. This plasmid was added xseAi for *P. putida* to pBBR1-P_{Rha}-BAS-xseBkt2440-P_{BAD}-Cas9-Km. The linear fragment digested (SacI) from pBBR1-P_{Rha}-BAS-Km-amp-ccdB, *xseB* gene, xseAi cassette synthesized from BGI and BAD-Cas9 cassette was co-transformed into GB05-dir and selected on LB plates containing 15 μg mL^{-1} kanamycin (37 °C) to assemble pBBR1-P_{Rha}-BAS-xseBkt2440-P_{BAD}-Cas9-xseAi-Km by LLHR.

RK2-P_{fapO}-GFP-genta-$FapR_{ecoli}$. RK2-P_{fapO}-GFP-genta-$fapR_{7029}$ This biosensor plasmid is based on an RK2 origin and harbors the *gfp* and gentamicin genes under the control of the J233 promoter and codon-optimized *fapR* gene for *E. coli*. The oriV (origin of replication) and trfA gene were amplified from RK2-apra-cm with primers rk2-1/rk2-2, the J233-GFP cassette was amplified from pBBR1-Rha-GFP-kan with primers J233-GFP-1/J233-GFP-2, the gentamicin resistance gene was amplified from R6K-loxM-genta with primers genta-1/genta-2, the $fapR_{ecoli}$ gene was synthesized by BGI (Supplementary Data 1), and the ampicillin resistance gene was amplified from R6K-amp-ccdB with primers amp-1/amp-2. These five fragments were co-transformed into GB05-dir induced for the expression of full-length RecE/RecT and selected on LB plates containing 100 μg ml^{-1} ampicillin (37 °C) for linear plus linear homologous recombination (LLHR) to assemble RK2-P_{fapO}-GFP-genta-$FapR_{ecoli}$. Construction of the expression plasmids RK2-P_{fapO}-GFP-genta-$FapR_{7029}$ and RK2-P_{fapO}-GFP-genta-$FapR_{kt2440}$ were the same as for RK2-P_{fapO}-GFP-genta-$FapR_{ecoli}$ except for using the codon-optimized *fapR* genes for *S. brevitalea* DSM7029 and *P. putida* KT2440.

p15A-cm-P_{tac}-T7-rppA. This plasmid is based on a p15A origin and harbors the *rppA* gene under the control of the tac-T7 promoter. A fragment containing the p15A origin and chloramphenicol resistance gene was amplified from p15A-cm[75] with primers p15A-cm-1/p15A-cm-2, and a fragment containing the tac-T7 promoter and *rppA* gene was synthesized by BGI (Supplementary Data 1). These two fragments were co-transformed into GB05-dir[75] and followed by selection on LB plates containing 15 μg mL^{-1} chloramphenicol for linear plus linear homologous recombination to generate p15A-cm-P_{tac}-T7-rppA.

p15A-cm-P_{tac}-T7-rpALS. This plasmid is based on a p15A origin and harbors the *rpALS* gene under the control of the tac-T7 promoter. A fragment containing the p15A origin and chloramphenicol resistance gene was amplified from p15A-cm[75] with primers p15A-cm-1/p15A-cm-2, and a fragment containing the tac-T7 promoter and *rpALS* gene was synthesized by BGI (Supplementary Data 1). These two fragments were co-transformed into GB05-dir[75] and followed by selection on LB plates containing 15 μg mL^{-1} chloramphenicol for linear plus linear homologous recombination to generate p15A-cm-P_{tac}-T7-rpALS.

pBeloBAC11-apra-epo-accA-pccB-tRNA-epi-matB-attP. This plasmid is based on a pBeloBAC11 origin and harbors the epothilone gene cluster, metabolic pathway element (accA-pccB-tRNA-epi-matB), and transposable element (int-attP). For the initial construct, the original pBeloBAC11-apra-epo-attP[61] was co-transformed with amp-ccdB amplified from R6K-amp-ccdB with primers BAC-amp-1/BAC-amp-2 into GBred-gyrA462[74] to generate pBeloBAC11-apra-epo-attP-amp-ccdB. Then, the pBeloBAC11-apra-epo-attP-amp-ccdB was digested with PacI, and the five fragments containing five metabolic pathway element genes were synthesized by BGI (Supplementary Data 1). These two fragments were co-transformed into GB05-dir[75] and followed by selection on LB plates containing 20 μg mL^{-1} apramycin to generate pBeloBAC11-apra-epo-accA-pccB-tRNA-epi-matB-attP.

Culture conditions

E. coli and mutants were cultured in Luria-Bertani (LB) broth or on LB agar plates (1.2% agar) with ampicillin (100 μg mL^{-1}), kanamycin (15 μg mL^{-1}), chloramphenicol (15 μg mL^{-1}) or gentamicin (5 μg mL^{-1}) as required. *S. brevitalea* DSM7029[46] and mutants were cultured in CYMG (8 g L^{-1} Casein peptone, 4 g L^{-1} Yeast extract, 4.06 g L^{-1} $MgCl_2{\cdot}2H_2O$, 5 mL L^{-1} glycerol) broth or agar plates with apramycin (20 μg mL^{-1}), kanamycin (20 μg mL^{-1}) or gentamicin (15 μg mL^{-1}) as required. *S. brevitalea* DSM7029 and mutants were also cultured in mixed cellulose medium (1 g L^{-1} CMC-Na, 1 g L^{-1} Avicel, 4 g L^{-1} K_2HPO_4, 2 g L^{-1} $(NH_4)_2SO_4$, 0.5 g L^{-1} $MgSO_4{\cdot}7H_2O$). Reagents were purchased from New England Biolabs, Thermo Fisher Scientific, Invitrogen, and Sigma-Aldrich. *P. putida* and mutants were cultured in Luria-Bertani (LB) broth or on LB agar plates (1.2% agar) with kanamycin (15 μg mL^{-1}), or gentamicin (10 μg mL^{-1}) as required.

Multiplex Genomic engineering

Methods to obtain dsDNA substrates for accurate editing of metabolic pathway genes and genome reduction genes in *E. coli* BL21 or *S. brevitalea* DSM7029. In *E. coli* BL21, for the key genes that need to be upregulated due to insufficient expression, the constitutive T7 promoter is adopted to replace the original promoter of the target genes. The T7 promoter cassette contains homologous arm sequences (HA_L and HA_R) with a length of 100 bp on both sides and T7 promoter (HA_L-T7-HA_R) with a length of 20 bp in the middle, and the total length of the T7 promoter cassette is 220 bp. For the key genes that need to be downregulated, the LVA protein degradation label is inserted after the coding sequence. The LVA protein degradation label cassette contains homologous arm sequences (HA_L and HA_R) with 100 bp length on both sides and the LVA protein degradation label (HA_L-LVA-HA_R) with 36 bp length in the middle, and the total length of the LVA protein degradation label cassette is 236 bp. For the key genes that need to be deleted, the region is replaced by the 30 bp non-coding sequence with 100 bp length homologous arm sequences (HA_L-non-coding-HA_R) on both sides. In *S. brevitalea* DSM7029, for upregulation genes, gentamicin promoter or endogenous constitutive promoter P37 in *S. brevitalea* DSM7029 was selected to construct the promoter cassette[72] (Supplementary Data 1). The genta resistance cassette

contains homologous arm sequences (HA_L and HA_R) with a length of 100 bp on both sides and gentamicin resistance gene (HA_L-genta-HA_R) with a length of 765 bp in the middle, and the total length of the genta cassette is 965 bp. The P37 cassette contains homologous arm sequences (HA_L and HA_R) with a length of 100 bp on both sides, and P37 (HA_L-P37-HA_R) with a length of 166 bp in the middle, and the total length of the P37-promoter cassette is 366 bp. For the downregulation genes, the LVA protein degradation label cassette and genome reduction strategy were the same with BL21. In *P. putida* KT2440, for upregulation genes, a gentamicin promoter was selected to construct the promoter cassette. The gentamicin promoter cassette contains homologous arm sequences (HA_L and HA_R) with a length of 100 bp on both sides and gentamicin promoter (HA_L-P_{genta}-HA_R) with a length of 233 bp in the middle, and the total length of gentamicin-promoter cassette is 433 bp. For the downregulation genes, the LVA protein degradation label cassette and genome reduction strategy were the same with BL21.

The establishment method of ReaL-MGE. The process of ReaL-MGE 1.0 using variant iv as an example: ReaL-MGE 1.0 assisted genome editing requires twice electroporations. The purpose of the first electroporation is genome engineering, Redαβ recombinases and XseB are induced to express before first electroporation, and the phosphorothioate gRNA-expression PCR fragments and recombination substrate are electroporated into cell. gRNA and recombination substrate are linked by the target sequence of gRNA which facilitates Cas9 to cleave the PCR fragment and release the substrate. After the first electroporation, cells were recovered in an antibiotic-free medium supplemented with 10 nM dNTP for 4 h to ensure adequate and efficient homologous recombination. Cas9 is induced to express in the first recovery phase for promoting recombination by causing dsDNA breaks, knocking out *xseA* and releasing dsDNA substrates. In second electroporation, only phosphorothioate gRNA-expressing PCR fragments were electroporated and followed by continued induction of Cas9 expressing in the second recovery phase, the role of CRISPR/Cas9 here is for counterselection.

The process of ReaL-MGE 2.0 using variant vii as an example: ReaL-MGE 2.0 assisted genome editing also requires twice electroporations. The purpose of the first electroporation is genome engineering, Redαβ7029 recombinases and XseB7029 are induced to express before first electroporation, and the phosphorothioate cas9-gRNA-expression PCR fragments and recombination substrates are electroporated into cell. *cas9* and gRNA are linked by a terminator. After the first electroporation, cells were recovered in an antibiotic-free medium supplemented with 10 nM dNTP for 8 h to ensure adequate and efficient homologous recombination. *cas9* is placed under a constitutive promoter to express in the first recovery phase for promoting recombination by causing dsDNA breaks and knocking out *xseA*. In second electroporation, only phosphorothioate cas9-gRNA-expressing PCR fragments were electroporated, the role of CRISPR/Cas9 here is for counterselection.

Three-region replacement in *E. coli* BL21 by ReaL-MGE. The cultivation and preparation methods of competent cells of *E. coli* BL21 (pBBR1-P_{Rha}-Redγβα-xseB-P_{BAD}-Cas9-Km) were the same as previously described[25]. The competent cells of 1.3 mL *E. coli* BL21 (the OD_{600} values before electroporation were ~0.8) were mixed with chloramphenicol resistance genes to target three different target regions (region A-C) for electroporation using an Eppendorf 2510 electroporator at 1350 V using 1 mm gap width cuvettes. Electroporated cells were incubated at 30 °C in 1.3 mL antibiotic-free LB liquid medium with 10 nM dNTPs (GC50), 950 rpm for 2 h, and L-arabinose was added to induce the expression of Cas9 during the first recovery. The competent cells were prepared as in the first round of electroporation. The competent cells were mixed with the gRNA mixtures to target three different target regions (region A-C) for electroporation. Electroporated cells were incubated at 30 °C in 1 mL antibiotic-free LB liquid medium, 950 rpm for 2 h, and Cas9 was induced during the second recovery before plating (LB, 15 μg mL^{-1} chloramphenicol). 192 clones were checked by colony PCR for each biological replicate.

The mutant library of the malonyl-CoA metabolic network was established by ReaL-MGE. The cultivation and preparation methods of competent cells of *E. coli* BL21 (pBBR1-P_{Rha}-Redγβα-xseB-P_{BAD}-Cas9-Km and RK2-J233-GFP-genta-FapRecoli-amp), *S. brevitalea* DSM7029 (pBBR1-P_{Rha}-Redγ-Redαβ7029-xseB7029-Km and RK2-J233-GFP-genta-FapR7029-amp) and *P. putida* KT2440 (pBBR1-P_{Rha}-BAS-xseBkt2440-P_{BAD}-Cas9-Km and RK2-J233-GFP-genta-FapRPp-amp) were the same as previously described[25,77]. The competent cells of 1.3 mL *E. coli* BL21 were mixed with dsDNA substrates (HA_L-T7-HA_R, HA_L-LVA-HA_R, and HA_L-noncoding-HA_R) and the gRNA mixtures for precisely targeted editing of key genes or regions for electroporation using an Eppendorf 2510 electroporator at 1350 V using 1 mm gap width cuvettes. Electroporated cells were incubated at 30 °C in 1.3 mL antibiotic-free LB liquid medium with 10 nM dNTPs (GC50), 950 rpm for 4 h, and L-arabinose was added to induce the expression of Cas9 during recombineering recovery. The competent cells were prepared as in the first round of electroporation. The competent cells were mixed with the gRNA mixtures to target key genes or regions for electroporation. Electroporated cells were incubated at 30 °C in 1 mL antibiotic-free LB liquid medium, 950 rpm for 8 h, and Cas9 was induced during recovery before plating (LB, 40 μg mL^{-1} gentamicin). The mutants with low yield of malonyl-CoA were cleared by resistance screening, and the fluorescence intensity of mutants was detected by Microplate Reader. The mutants with higher fluorescence intensity were extracted and detected for intracellular malonyl-CoA concentration to confirm the correlation between fluorescence intensity and intracellular malonyl-CoA concentration. Genotypes of mutants with the highest intracellular malonyl-CoA concentration were detected to identify the key genes and genome reduction strategy for improving intracellular malonyl-CoA concentration by colony PCR. The mutant library of malonyl-CoA metabolic network and genome reduction strategy in *S. brevitalea* DSM7029 was similar to that in BL21. In the first round of electroporation in DSM 7029, Cas9 + gRNA mixtures should be added in addition to the substrates. Electroporated cells were incubated at 22 °C in 1.3 mL antibiotic-free CYMG liquid medium with 10 nM dNTPs (GC50), 950 rpm for 8 h. Then the competent cells were mixed with the Cas9 + gRNA mixtures for electroporation. Electroporated cells were incubated at 30 °C in 1 mL antibiotic-free CYMG liquid medium, 950 rpm for 12 h before plating (CYMG, 100 μg mL^{-1} gentamicin). Malonyl-CoA detection and identification of key genes were the same as in *E. coli* BL21. The mutant library of malonyl-CoA metabolic network and genome reduction strategy in *P. putida* KT2440 was similar to that in BL21. After the first round electroporation, electroporated cells were incubated at 22 °C in 1.3 mL antibiotic-free LB liquid medium with 10 nM dNTPs, 950 rpm for 4 h. After the second round electroporation, electroporated cells were incubated at 22 °C in 1.3 mL antibiotic-free LB liquid medium, 950 rpm for 8 h. Malonyl-CoA detection and identification of key genes were the same as in *E. coli* BL21.

***P. putida* strain culture and transformation.** *P. putida* strains were cultured at 30 °C. *P. putida* strains in this study were transformed by electroporation as previously described[77].

Malonyl-CoA quantification. The extraction and quantification of malonyl-CoA were implemented as previous[35]. The culture to be tested was cultured to an OD_{600} of 0.4, and 1.8 mL of the culture was chilled in ice and centrifuged at 4000 × *g* and 4 °C for 15 min. After washing with PBS, 120 μL of lysis buffer (45:45:10 acetonitrile: methanol: water with 0.1 M formic acid) was added to ice and

vigorously vortexing. The extract was incubated in ice by intermittent vortexing for 15 min. After 15 min, ammonium hydroxide was added to neutralize the previous acetic acid and centrifuged at 15000 × *g* and 4 °C for 3 min. The supernatant was analyzed by LC-MS. Standard analysis of prepared samples was measured on an LC-DAD system coupled to a Bruker Impact HD microTOF Q III ESI-MS ion trap instrument operating in positive ionization mode. The chromatographic conditions were: Thermo™ Acclaim™ RSLC 120 C_{18} column, 100 by 2.1 mm, 2.2 µm particle size. Solvent gradient (with solvents A [10 mM tributylamine, 15 mM acetic acid and 5% methanol in distilled water] and B [isopropyl alcohol]) from 0% B at 0 min to 0% B at 0.5 min, 0% B at 0.5 min to 12% B at 1.5 min, 12% B at 1.5 min to 27.5% B at 10 min, 27.5% B at 10 min to 90% B at 20 min, 90% B at 20 min to 90% B at 25 min, 90% B at 25 min to 0% B at 28 min, 0% B at 28 min to 0% B at 35 min at a flow rate of 0.3 mL min^{-1}. Detection was recorded by both the diode array and ESI-MS.

Colony PCR and sequencing. The colonies were inoculated from plates into 1 mL medium supplemented with appropriate antibiotics, and suspended in 1 mL ddH_2O. After heating at 95 °C for 15 min, a 1 µL boiled sample was used as a PCR template. Analytical PCR primers were designed to amplify 0.5–1.5 kb across replacement junctions (Supplementary Data 2). The *E. coli* BL21.C33 was sequenced completely, and the genome sequence login number in NCBI is PRJNA1161194. The *S. brevitalea* DSM7029Δglb.C21 was sequenced completely, and the genome sequence login number in NCBI is PRJNA1161196. The *S. brevitalea* DSM7029Δglb.C21:: lignocellulose was sequenced completely, and the genome sequence login number in NCBI is PRJNA1161198. The *P. putida*.C177 was sequenced completely, and the genome sequence login number in NCBI is PRJNA1160430.

Flow Cytometry for bacteria. The strains to be analyzed were inoculated from glycerin stock onto growth medium plates. Incubate the plates at the optimum growth temperature of the strain until colonies form. The colonies were scraped and cultured in the liquid medium to OD_{600} = 0.8. For each fixed sample, 1.5 mL PBS solution was added for fixation. 1.5 mL fixative was added into the 2 mL reaction tube, vortex mixing was performed, centrifuged at 12,500 × *g* for 5 min, and the supernatant was discarded at 4 °C. Repeat before using it. Fill the flow cytometer sheath solution and empty the waste container. Perform flow cytometer start-up and quality control procedures. The prepared bacterial suspension was transferred to a tube suitable for the flow cytometer sample port. Prepare acquisition diagrams for FSC and SSC in the software. The sample was measured in flow cytometer setting mode, and the gain Settings of the FSC and SSC were adjusted to ensure that the entire population was visible. Bacterial populations were gated, and duplicates were distinguished by mapping FSC-Area (FSC-A) and FSC-Height (FSC-H). The acquisition map was prepared for fluorescence parameters, i.e., histograms of fluorescence measurements of the mutant strain expressing GFP and the respective wild-type strain. Start collecting samples in Set mode and adjust the gain setting of the acquisition channel. Start measuring samples, recording at least 10,000 events, and saving all measurements. For cell sorting, specify the sort gate and collection mode. For unit sorting, install the collection pipe and begin sorting. After sorting out a cell population, the sample inlet and flow cells were cleaned using a rinse and cleaning agent recommended by the flow cytometer supplier. Run the sample in collection mode with PBS solution for 2 min to check the remaining cells in the system. Repeat the cleaning flow cell if more than 50 events are recorded in the cell gate. Perform flow cytometer shutdown procedure to clean flow cells.

Cell morphology determination by using the field emission scanning electron microscopy (FESEM)

A large number of samples were centrifuged at 5000 rpm for 2 min, and the supernatant was removed. 1 × PBS (PH = 7.4) was added for cleaning. The samples were left standing for 15 min and centrifuged at 5000 × *g* for 2 min, and the supernatant was removed. 2.5% glutaraldehyde (1 × PBS) was added and fixed at 4 °C for 3 h, centrifuged at 5000 × *g* for 2 min, and the supernatant was removed. The supernatant was cleaned three times with 1X PBS for 15 min each time. The samples were dehydrated with an aqueous ethanol solution according to the concentration gradient of 30, 50, 70, 80, and 90%. Each step was about 15 min. The supernatant was discarded, and then the samples were dehydrated in 100% ethanol for 15 min twice. The sample was suspended by shock, and the suspended droplets of bacteria were absorbed into the cover glass. The cover glass containing the sample was dried in a critical point dryer. After thoroughly drying the sample, the cover glass was adhered to the sample table with conductive tape and gilded. Finally, they were observed under an electron microscope.

Efficient expression of flaviolin, aloesone and epothilone

The flaviolin gene (*rppA*) was placed on the p15A plasmid under the control of the tac-T7 promoter, and the plasmid was transformed into an optimal *E. coli* BL21 mutant. The yield of flaviolin was measured by fermentation. The expression of aloesone was the same with flaviolin.

Epothilone gene cluster was placed on the single copy plasmid BAC, and resistance screening marker (*apra*) and site-specific recombinase gene cassette (*attP*-int) were placed on the BAC. In the modified *S. brevitalea* DSM7029 that replaced the glidobactin gene cluster with *attB* site, where the key genes that improved intracellular malonyl-CoA concentration were selected for strong promoter replacement, protein degradation tags were added to construct the chassis mutant and the genome reduction strategy was implemented. The epothilone gene cluster was transferred into the *S. brevitalea* DSM7029 genome by site-specific recombination, and the yield of epothilone was measured by fermentation.

Extraction and analysis of the fermentation extracts

For flaviolin, M9 minimal medium (20 g L^{-1} glucose, 12.8 g L^{-1} $Na_2HPO_4{\cdot}7H_2O$, 3 g L^{-1} KH_2PO_4, 0.5 g L^{-1} NaCl, 1 g L^{-1} NH_4Cl, 2 mM $MgSO_4$, 0.1 mM $CaCl_2$) was used. *E. coli* BL21 mutants with p15A-cm-tac-T7-rppA plasmid were inoculated from colonies on LB agar plates into 1.3 mL LB medium supplemented with appropriate antibiotics and were cultivated at 37 °C, 950 rpm overnight. Then, 1 mL aliquot of seed culture was transferred into 250 ml flasks containing 50 ml M9 minimal medium with shaking at 37 °C, 200 rpm. When the OD_{600} was around 0.8, the culture was induced with 0.5 mM isopropyl β-D-1-thiogalactopyranoside (IPTG) and cultivated for 48 h at 30 °C, 200 rpm. For the analysis of flaviolin, culture supernatant was filtrated through 0.22 µm PVDF syringe filters. The analysis instruments were the same as malonyl-CoA. Solvent gradient (with solvents A [water and 0.1% of formic acid] and B [acetonitrile and 0.1% of formic acid]) from 5% B at 1 min to 70% B at 15 min, 70% B at 15 min to 100% B at 20 min at a flow rate of 0.3 mL min^{-1}. Detection was recorded by both the diode array and ESI-MS. For aloesone, R/2 medium (3 g L^{-1} yeast extract, 6.75 g L^{-1} KH_2PO_4, 2 g L^{-1} $(NH_4)_2HPO_4$, 0.8 g L^{-1} $MgSO_4$, 3 g L^{-1} $(NH_4)_2SO_4$, 0.85 g L^{-1} citric acid, 20 g L^{-1} glucose, 5 mL L^{-1} TMS. The TMS contains 10 g L^{-1} $FeSO_4{\cdot}7H_2O$, 2.25 g L^{-1} $ZnSO_4{\cdot}7H_2O$, 0.58 g L^{-1} $MnSO_4{\cdot}5H_2O$, 1 g L^{-1} $CuSO_4{\cdot}5H_2O$, 0.1 g L^{-1} $(NH_4)_6Mo_7O_{24}{\cdot}4H_2O$, 0.02 g L^{-1} $Na_2B_4O_7{\cdot}10H_2O$, 2 g L^{-1} $CaCl_2{\cdot}2H_2O$ in 0.1 M HCl.) was used. The extraction and analysis were the same as flaviolin.

For epothilone, the *S. brevitalea* DSM7029 mutants were inoculated from colonies on CYMG agar plates into 1.3 mL CYMG medium supplemented with appropriate antibiotics, and were cultivated at 30 °C, 950 rpm overnight. Then, 1 mL aliquot of seed culture was transferred into 250 ml flasks containing 50 mL CYMG

medium with shaking for 48 h at 30 °C, 200 rpm. Then resins XAD-16 (2%) were added, and continually incubated for another 48 h. The resin and biomass were harvested by centrifugation and then extracted with 40 mL methanol later. The extracts were concentrated *in vacuo* to dryness and dissolved in 1 mL of methanol before analysis by LC/MS. The analysis instruments were the same as flaviolin and aloesone. The gradient was applied: 5% B at 5 min to 95% B within 20 min, followed by 5 min with 95% B at a flow rate of 0.3 mL min^{-1}.

Statistics & reproducibility

Statistical analysis was performed by GraphPad Prism 10.0. Two groups were analyzed by two-sided unpaired Student's *t* test. Three or more groups were analyzed by One-way ANOVA with Dunnett's multiple comparisons test. Data was presented as mean values ± SD. *P*-value < 0.05 was considered a significant difference. No data was excluded from the analyses. Details of the biological replicates were provided in figure legends wherever necessary.

Reporting summary

Further information on research design is available in the Nature Portfolio Reporting Summary linked to this article.

Data availability

Data supporting the findings of this work are available within the paper and its Supplementary Information files. A reporting summary for this Article is available as a Supplementary Information file. The *E. coli* BL21.C33 genome sequence login number in NCBI is PRJNA1161194. The *S. brevitalea* DSM7029Δglb.C21 genome sequence login number in NCBI is PRJNA1161196. The *S. brevitalea* DSM7029Δglb.C21:: lignocellulose genome sequence login number in NCBI is PRJNA1161198. The *P. putida*.C177 genome sequence login number in NCBI is PRJNA1160177. Source data are provided in this paper.

References

1. Huo, L. et al. Heterologous expression of bacterial natural product biosynthetic pathways. *Nat. Prod. Rep.* **36**, 1412–1436 (2019).
2. Zhang, J. J., Tang, X. Y., Zhang, M., Nguyen, D. & Moore, B. S. Broad-host-range expression reveals native and host regulatory elements that influence heterologous antibiotic production in gram-negative bacteria. *mBio* **8**, e01291–01217 (2017).
3. Song, C. W., Lee, J. & Lee, S. Y. Genome engineering and gene expression control for bacterial strain development. *Biotechnol. J.* **10**, 56–68 (2015).
4. Cao, M. F., Tran & Zhao, H. M. Unlocking nature's biosynthetic potential by directed genome evolution. *Curr. Opin. Biotechnol.* **66**, 95–104 (2020).
5. Calero, P. & Nikel, P. I. Chasing bacterial chassis for metabolic engineering: a perspective review from classical to non-traditional microorganisms. *Microb. Biotechnol.* **12**, 98–124 (2019).
6. Oyetunde, T., Bao, F. S., Chen, J. W., Martin, H. G. & Tang, Y. J. J. Leveraging knowledge engineering and machine learning for microbial bio-manufacturing. *Biotechnol. Adv.* **36**, 1308–1315 (2018).
7. Gu, C. D., Kim, G. B., Kim, W. J., Kim, H. U. & Lee, S. Y. Current status and applications of genome-scale metabolic models. *Genome Biol.* **20**, 121 (2019).
8. Wei, L. et al. Regulation by competition: a hidden layer of gene regulatory network. *Quant. Biol.* **7**, 110–121 (2019).
9. Lawson, C. E. et al. Machine learning for metabolic engineering: A review. *Metab. Eng.* **63**, 34–60 (2021).
10. Csorgo, B., Nyerges, A. & Pal, C. Targeted mutagenesis of multiple chromosomal regions in microbes. *Curr. Opin. Microbiol.* **57**, 22–30 (2020).
11. Jiang, W. Y., Bikard, D., Cox, D., Zhang, F. & Marraffini, L. A. RNA-guided editing of bacterial genomes using CRISPR-Cas systems. *Nat. Biotechnol.* **31**, 233–239 (2013).
12. Ciaccia, P. N., Liang, Z., Schweitzer, A. Y., Metzner, E. & Isaacs, F. J. Enhanced eMAGE applied to identify genetic factors of nuclear hormone receptor dysfunction via combinatorial gene editing. *Nat. Commun.* **15**, 5218 (2024).
13. Zhang, Y. M., Buchholz, F., Muyrers, J. P. P. & Stewart, A. F. A new logic for DNA engineering using recombination in Escherichia coli. *Nat. Genet.* **20**, 123–128 (1998).
14. Muyrers, J. P. P., Zhang, Y. M., Testa, G. & Stewart, A. F. Rapid modification of bacterial artificial chromosomes by ET-recombination. *Nucleic Acids Res.* **27**, 1555–1557 (1999).
15. Zhang, Y. M., Muyrers, J. P. P., Testa, G. & Stewart, A. F. DNA cloning by homologous recombination in Escherichia coli. *Nat. Biotechnol.* **18**, 1314–1317 (2000).
16. Muyrers, J. P. P., Zhang, Y. M., Buchholz, F. & Stewart, A. F. RecE/RecT and Red alpha/Red beta initiate double-stranded break repair by specifically interacting with their respective partners. *Genes Dev.* **14**, 1971–1982 (2000).
17. Ellis, H. M., Yu, D. G., DiTizio, T. & Court, D. L. High efficiency mutagenesis, repair, and engineering of chromosomal DNA using single-stranded oligonucleotides. *Proc. Natl. Acad. Sci. USA* **98**, 6742–6746 (2001).
18. Zhang, Y. M., Muyrers, J. P. P., Rientjes, J. & Stewart, F. Phage annealing proteins promote oligonucleotide-directed mutagenesis in Escherichia coli and mouse ES cells. *Bmc Mol. Biol.* **4**, 1 (2003).
19. Wang, H. H. et al. Programming cells by multiplex genome engineering and accelerated evolution. *Nature* **460**, 894–898 (2009).
20. Wang, H. H. et al. Genome-scale promoter engineering by coselection MAGE. *Nat. Methods* **9**, 591–593 (2012).
21. Warner, J. R., Reeder, P. J., Karimpour-Fard, A., Woodruff, L. B. A. & Gill, R. T. Rapid profiling of a microbial genome using mixtures of barcoded oligonucleotides. *Nat. Biotechnol.* **28**, 856–862 (2010).
22. Nyerges, A. et al. A highly precise and portable genome engineering method allows comparison of mutational effects across bacterial species. *Proc. Natl. Acad. Sci. USA* **113**, 2502–2507 (2016).
23. Nyerges, A. et al. Directed evolution of multiple genomic loci allows the prediction of antibiotic resistance. *Proc. Natl. Acad. Sci. USA* **115**, E5726–E5735 (2018).
24. Wannier, T. M. et al. GM. Recombineering and MAGE. *Nat. Rev. Methods Prim.* **1**, 7 (2021).
25. Wang, X. et al. Improved dsDNA recombineering enables versatile multiplex genome engineering of kilobase-scale sequences in diverse bacteria. *Nucleic Acids Res.* **50**, e15 (2021).
26. Rostain, W. et al. Cas9 off-target binding to the promoter of bacterial genes leads to silencing and toxicity. *Nucleic Acids Res.* **51**, 3485–3496 (2023).
27. Zhang, Y. et al. A gRNA-tRNA array for CRISPR-Cas9 based rapid multiplexed genome editing in Saccharomyces cerevisiae. *Nat. Commun.* **10**, 1053 (2019).
28. Sharda, M., Badrinarayanan, A. & Seshasayee, A. S. N. Evolutionary and comparative analysis of bacterial nonhomologous end joining repair. *Genome Biol. Evol.* **12**, 2450–2466 (2020).
29. Ronda, C., Pedersen, L. E., Sommer, M. O. A. & Nielsen, A. T. CRMAGE: CRISPR optimized MAGE recombineering. *Sci. Rep.* **6**, 19452 (2016).
30. Garst, A. D. et al. Genome-wide mapping of mutations at single-nucleotide resolution for protein, metabolic and genome engineering. *Nat. Biotechnol.* **35**, 48–55 (2017).
31. Reisch, C. R. & Prather, K. L. J. Scarless cas9 assisted recombineering (no-SCAR) in escherichia coli, an easy-to-use system for genome editing. *Curr. Protoc. Mol. Biol.* **117**, 1–20 (2017).
32. Tee, T. W., Chowdhury, A., Maranas, C. D. & Shanks, J. V. Systems metabolic engineering design: Fatty acid production as an

emerging case study. *Biotechnol. Bioeng.* **111**, 849–857 (2014).
33. Xu, P., Qiao, K. J., Ahn, W. S. & Stephanopoulos, G. Engineering Yarrowia lipolytica as a platform for synthesis of drop-in transportation fuels and oleochemicals. *Proc. Natl Acad. Sci. USA* **113**, 10848–10853 (2016).
34. Liu, H., Marsafari, M., Wang, F., Deng, L. & Xu, P. Engineering acetyl-CoA metabolic shortcut for eco-friendly production of polyketides triacetic acid lactone in Yarrowia lipolytica. *Metab. Eng.* **56**, 60–68 (2019).
35. Yan, D. et al. Repurposing type III polyketide synthase as a malonyl-CoA biosensor for metabolic engineering in bacteria. *Proc. Natl. Acad. Sci. USA* **115**, 9835–9844 (2018).
36. Bian, X. et al. Heterologous production of glidobactins/luminmycins in Escherichia coli Nissle containing the glidobactin biosynthetic gene cluster from Burkholderia DSM7029. *Chembiochem* **15**, 2221–2224 (2014).
37. Bian, X. et al. Heterologous production and yield improvement of epothilones in burkholderiales strain DSM 7029. *ACS Chem. Biol.* **12**, 1805–1812 (2017).
38. Davis, M. S., Solbiati, J. & Cronan, J. E. Overproduction of acetyl-CoA carboxylase activity increases the rate of fatty acid biosynthesis in Escherichia coli. *J. Biol. Chem.* **275**, 28593–28598 (2000).
39. Zha, W., Rubin-Pitel, S. B., Shao, Z. & Zhao, H. Improving cellular malonyl-CoA level in Escherichia coli via metabolic engineering. *Metab. Eng.* **11**, 192–198 (2009).
40. Xu, P., Ranganathan, S., Fowler, Z. L., Maranas, C. D. & Koffas, M. A. G. Genome-scale metabolic network modeling results in minimal interventions that cooperatively force carbon flux towards malonyl-CoA. *Metab. Eng.* **13**, 578–587 (2011).
41. Lian, J., Si, T., Nair, N. U. & Zhao, H. Design and construction of acetyl-CoA overproducing Saccharomyces cerevisiae strains. *Metab. Eng.* **24**, 139–149 (2014).
42. Wu, J., Zhang, X., Xia, X. & Dong, M. A systematic optimization of medium chain fatty acid biosynthesis via the reverse beta-oxidation cycle in Escherichia coli. *Metab. Eng.* **41**, 115–124 (2017).
43. Milke, L., Kallscheuer, N., Kappelmann, J. & Marienhagen, J. Tailoring Corynebacterium glutamicum towards increased malonyl-CoA availability for efficient synthesis of the plant pentaketide noreugenin. *Micro. Cell Fact.* **18**, 71 (2019).
44. Zhang, S. et al. Metabolic engineering for efficient supply of acetyl-CoA from different carbon sources in Escherichia coli. *Micro. Cell Fact.* **18**, 130 (2019).
45. Hirokawa, Y., Kubo, T., Soma, Y., Saruta, F. & Hanai, T. Enhancement of acetyl-CoA flux for photosynthetic chemical production by pyruvate dehydrogenase complex overexpression in Synechococcus elongatus PCC 7942. *Metab. Eng.* **57**, 23–30 (2020).
46. Tang, B. et al. Reclassification of 'Polyangium brachysporum' DSM 7029 as Schlegelella brevitalea sp. nov. *Int. J. Syst. Evol. Microbiol.* **69**, 2877–2883 (2019).
47. Song, L., Ouedraogo, J. P., Kolbusz, M., Nguyen, T. T. M. & Tsang, A. Efficient genome editing using tRNA promoter-driven CRISPR/Cas9 gRNA in Aspergillus niger. *PLoS ONE* **13**, e0202868 (2018).
48. Easmin, F. et al. gRNA-transient expression system for simplified gRNA delivery in CRISPR/Cas9 genome editing. *J. Biosci. Bioeng.* **128**, 373–378 (2019).
49. Ploessl, D. et al. A repackaged CRISPR platform increases homology-directed repair for yeast engineering. *Nat. Chem. Biol.* **18**, 38–46 (2022).
50. Banno, S., Nishida, K., Arazoe, T., Mitsunobu, H. & Kondo, A. Deaminase-mediated multiplex genome editing in Escherichia coli. *Nat. Microbiol.* **3**, 423–429 (2018).
51. Maresca, M. et al. Single-stranded heteroduplex intermediates in lambda Red homologous recombination. *BMC Mol. Biol.* **11**, 54 (2010).
52. Mosberg, J. A., Lajoie, M. J. & Church, G. M. Lambda red recombineering in escherichia coli occurs through a fully single-stranded intermediate. *Genetics* **186**, 791–799 (2010).
53. Jung, H., Liang, J., Jung, Y. & Lim, D. Characterization of cell death in Escherichia coli mediated by XseA, a large subunit of exonuclease VII. *J. Microbiol.* **53**, 820–828 (2015).
54. Mosberg, J. A., Gregg, C. J., Lajoie, M. J., Wang, H. H. & Church, G. M. Improving lambda red genome engineering in Escherichia coli via rational removal of endogenous nucleases. *PLoS ONE* **7**, e44638 (2012).
55. Schujman, G. E., Altabe, S. & de Mendoza, D. A malonyl-CoA-dependent switch in the bacterial response to a dysfunction of lipid metabolism. *Mol. Microbiol.* **68**, 987–996 (2008).
56. Chen, X. X., Yang, X. Y., Shen, Y., Hou, J. & Bao, X. M. Increasing malonyl-CoA derived product through controlling the transcription regulators of phospholipid synthesis in saccharomyces cerevisiae. *Acs Synth. Biol.* **6**, 905–912 (2017).
57. Yang, Y., Lin, Y., Li, L., Linhardt, R. J. & Yan, Y. Regulating malonyl-CoA metabolism via synthetic antisense RNAs for enhanced biosynthesis of natural products. *Metab. Eng.* **29**, 217–226 (2015).
58. Wu, J. J., Yu, O., Du, G. C., Zhou, J. W. & Chen, J. Fine-tuning of the fatty acid pathway by synthetic antisense RNA for enhanced (2S)-naringenin production from L-tyrosine in Escherichia coli. *Appl. Environ. Microbiol.* **80**, 7283–7292 (2014).
59. Carbonell, P. et al. An automated Design-Build-Test-Learn pipeline for enhanced microbial production of fine chemicals. *Commun. Biol.* **1**, 66 (2018).
60. Wang, Y. P., San, K. Y. & Bennett, G. N. Cofactor engineering for advancing chemical biotechnology. *Curr. Opin. Biotechnol.* **24**, 994–999 (2013).
61. Liu, J. et al. Rational construction of genome-reduced Burkholderiales chassis facilitates efficient heterologous production of natural products from proteobacteria. *Nat. Commun.* **12**, 4347 (2021).
62. Liu, J., Wang, X., Dai, G., Zhang, Y. & Bian, X. Microbial chassis engineering drives heterologous production of complex secondary metabolites. *Biotechnol. Adv.* **59**, 107966 (2022).
63. Posfai, G. et al. Emergent properties of reduced-genome Escherichia coli. *Science* **312**, 1044–1046 (2006).
64. Frost, L. S., Leplae, R., Summers, A. O. & Toussaint, A. Mobile genetic elements: the agents of open source evolution. *Nat. Rev. Microbiol.* **3**, 722–732 (2005).
65. Martinez-Garcia, E., Nikel, P. I., Aparicio, T. & de Lorenzo, V. Pseudomonas 2.0: genetic upgrading of P. putida KT2440 as an enhanced host for heterologous gene expression. *Micro. Cell Fact.* **13**, 159 (2014).
66. Zhang, N. et al. Self-controlled in silico gene knockdown strategies to enhance the sustainable production of heterologous terpenoid by Saccharomyces cerevisiae. *Metab. Eng.* **83**, 172–182 (2024).
67. Qiu, C. et al. Biosensor-coupled in vivo mutagenesis and omics analysis reveals reduced lysine and arginine synthesis to improve malonyl-coenzyme a flux in Saccharomyces cerevisiae. *mSystems* **7**, e0136621 (2022).
68. Whitford, C. M. et al. Systems analysis of highly multiplexed CRISPR-Base editing in streptomycetes. *ACS Synth. Biol.* **12**, 2353–2366 (2023).
69. Huang, K., Zhang, B., Chen, Y., Liu, Z. Q. & Zheng, Y. G. Comparative transcriptome analysis of streptomyces nodosus mutant with a high-yield amphotericin B. *Front. Bioeng. Biotechnol.* **8**, 621431 (2020).
70. Liu, M. et al. Improving the production of acetyl-CoA-derived chemicals in Escherichia coli BL21(DE3) through iclR and arcA deletion. *BMC Microbiol.* **17**, 10 (2017).
71. Yu, Y. et al. Reassembly of the biosynthetic gene cluster enables high epothilone yield in engineered schlegelella brevitalea. *ACS Synth. Biol.* **9**, 2009–2022 (2020).

72. Ouyang, Q. et al. Promoter screening facilitates heterologous production of complex secondary metabolites in burkholderiales strains. *ACS Synth. Biol.* **9**, 457–460 (2020).
73. Bhan, N., Xu, P., Khalidi, O. & Koffas, M. A. G. Redirecting carbon flux into malonyl-CoA to improve resveratrol titers: Proof of concept for genetic interventions predicted by OptForce computational framework. *Chem. Eng. Sci.* **103**, 109–114 (2013).
74. Wang, H. L. et al. Improved seamless mutagenesis by recombineering using ccdB for counterselection. *Nucleic Acids Res.* **42**, e37 (2014).
75. Fu, J. et al. Full-length RecE enhances linear-linear homologous recombination and facilitates direct cloning for bioprospecting. *Nat. Biotechnol.* **30**, 440–446 (2012).
76. Wang, H. L. et al. RecET direct cloning and Red alpha beta recombineering of biosynthetic gene clusters, large operons or single genes for heterologous expression. *Nat. Protoc.* **11**, 1175–1190 (2016).
77. Yin, J. et al. Single-stranded DNA-binding protein and exogenous RecBCD inhibitors enhance phage-derived homologous recombination in pseudomonas. *iScience* **14**, 1–14 (2019).

Acknowledgements

This work was supported by the National Key R&D Program of China (No. 2022YFA1304000 [X.W.]), the National Natural Science Foundation of China (32001059 [X.W.]), the National Natural Science Foundation of Shandong province (ZR2023YQ028 [X.W.]), Taishan Scholar Program of Shandong Province in China (tsqn202312007 [X.W.]) the Shandong Provincial Natural Science Foundation (ZR2022QC107 [W.Z.]), the Shenzhen Fundamental Research Program (2022A1515110795 [W.Z.]), the Natural Science Foundation of Jiangsu Province (BK20230253 [W.Z.]), the China Postdoctoral Science Foundation (2022M711925 [W.Z.], 2023T160386 [W.Z.]), the 111 project (B16030 [Y.Z.]), Major basic research project of Hunan Province (2024JC0007 [Y.Y.]), SKLMT Frontiers and Challenges Project [X.W.] of Shandong University and Fundamental Research Funds (2023QNTD001 [X.B.]) of Shandong University. AFS was funded by the Deutsche Forschungsgemeinschaft grant STE 903/6–1 [A.F.S.]. We thank Jingyao Qu and Haiyan Yu from the State Key Laboratory of Microbial Technology of SDU for LC-MS and FCS.

Author contributions

W.Z., X.W., X.B., and Y.Z. conceived the study; W.Z., X.W., Y.Z., Y.Y., and X.B. supervised the experiments; W.Z., Y.W., J.C., G.G., and Y.L. performed the experiments; W.Z., X.W., Y.W., J.C., G.G., J.H., Q.T., Y.Z., and X.B. analyzed data; X.W., A.F.S., and W.Z. wrote the manuscript with the input from all authors.

Competing interests

The authors declare no competing interests.

Additional information

Supplementary information The online version contains supplementary material available at https://doi.org/10.1038/s41467-024-54191-4.

Correspondence and requests for materials should be addressed to A. Francis Stewart, Youming Zhang, Xiaoying Bian or Xue Wang.

Peer review information *Nature Communications* thanks the anonymous reviewers for their contribution to the peer review of this work. A peer review file is available.